

## Over 17% efficiency all-small-molecule organic solar cells based on an organic molecular donor employing 2D side chain symmetric-breaking strategy

Zhiya Li,<sup>‡a</sup> Xunchang Wang,<sup>‡\*ab</sup> Nan Zheng,<sup>c</sup> Aziz Saporbaev,<sup>d</sup> Jiayi Zhang,<sup>a</sup> Cong Xiao,<sup>a</sup> Shiyun Lei,<sup>a</sup> Xufan Zheng,<sup>a</sup> Manxue Zhang,<sup>a</sup> Yuda Li,<sup>e</sup> Biao Xiao,<sup>a</sup> Renqiang Yang<sup>\*a</sup>

<sup>a</sup> Key Laboratory of Optoelectronic Chemical Materials and Devices (Ministry of Education), School of Optoelectronic Materials & Technology, Jiangnan University, Wuhan 430056, China.

<sup>b</sup> State Key Laboratory of Fine Blasting, Jiangnan University, Wuhan 430056, China

<sup>c</sup> Institute of Polymer Optoelectronic Materials and Devices, State Key Laboratory of Luminescent Materials and Devices, South China University of Technology, Guangzhou 510640, China

<sup>d</sup> Institute of Ion-plasma and Laser Technologies, National University of Uzbekistan, Uzbekistan

<sup>e</sup> Key Laboratory for Green Chemical Process of Ministry of Education, Wuhan Institute of Technology, Wuhan 430205, China.

\* E-mail:

wangxc@jhun.edu.cn (X. Wang)

yangrq@jhun.edu.cn (R. Yang)

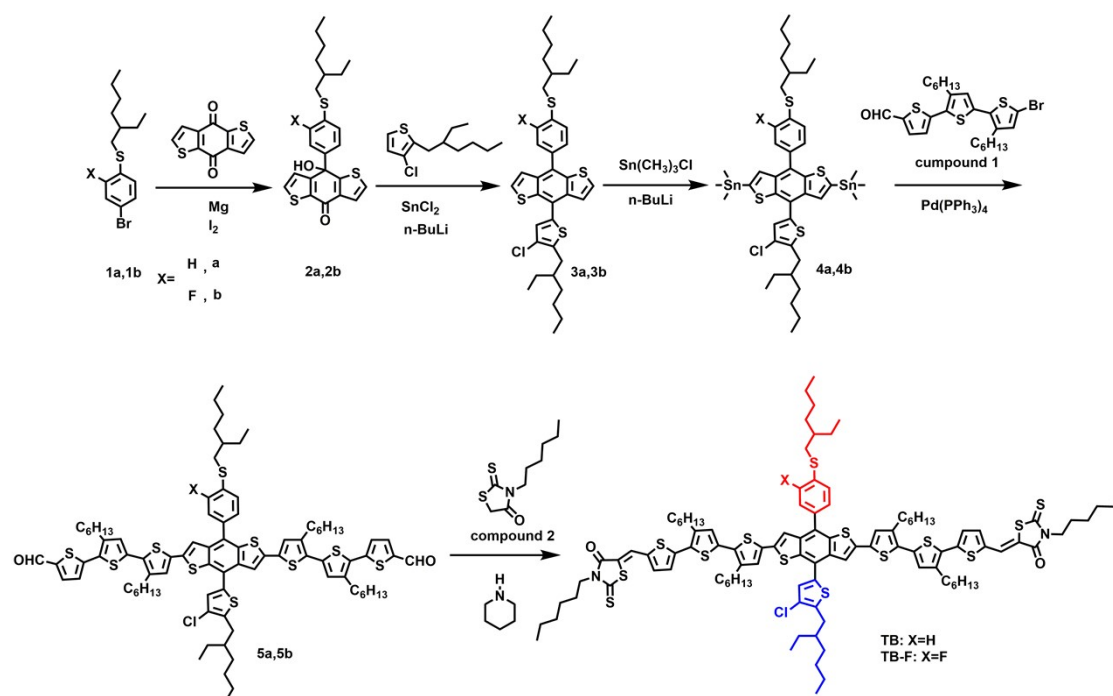
## **Contents**

1. Materials and Methods
2. Materials Synthesis
3. Reported High-performance ASM-OSCs
4. Density Functional Theory Calculation
5. UV-Vis Absorption
6. Cyclic Voltammetry
7. Ultraviolet Photoelectron Spectroscopy
8. Contact Angle
9. Grazing Incidence Wide-angle X-Ray Scattering
10. Solar Cell Device Fabrication and Characterization
11. Space-Charge-Limited Current Measurements
12. Dielectric Constant Measurements
13. Femtosecond Transient Absorption Spectroscopy Measurements
14. Atomic Force Microscopy
15. Transmission Electronic Microscopy
16. Binding Energy and D/A Molecular Stacking Calculation
17. In-depth X-ray Photoelectron Spectroscopy Measurement
18. Molecular Dynamic Analysis

## 1. Materials and Methods

All the reagents, unless otherwise specified, were purchased from Sigma-Aldrich Co., J&K, and Tokyo Chemical Industry Co., Ltd., and were used without further purification. Compounds L8-Bo, BTR-Cl, PDIN-F3N were purchased from Solarmer Materials Inc. Compound 1a and Compound 1b were synthesized by the reported method.<sup>[1]</sup>

## 2. Materials Synthesis



**Scheme S1.** The synthetic routes of TB and TB-F.

### *Synthesis of compound 2a and 2b*

The compound 1a (or 1b) (10 g, 33.22 mmol) and magnesium powder (0.956 g, 39.86 mmol) were added into dry THF (50 mL). Subsequently, the catalyst amount of I<sub>2</sub> (20 mg) was added as an initiator to the flask. The reaction mixture was refluxed at 70 °C for 4h until magnesium was completely consumed. After the reaction is cooled to room temperature, the Grignard reagent is obtained, then, transfer the freshly prepared Grignard reagent to the drip Funnel and slowly drop to benzo[1,2-b:4,5-b']dithiophene-

4,8-dione (6.3 g, 28.6 mmol) which was dispersed in 150 mL toluene. Subsequently, the mixture was stirred overnight in room temperature. Then it was extracted with dichloromethane and washed by water three times, dried over MgSO<sub>4</sub> to remove water, and purified by column chromatography (eluent: petroleum ether) to obtain light white solid.

**2a:** 8.29 g, yield: 67%. <sup>1</sup>H NMR (400 MHz, CDCl<sub>3</sub>) δ (ppm): 7.56 (d, 1H), 7.33 (d, 1H), 7.28 (s, 1H), 7.26-7.24 (m, 2H), 7.21 (d, 2H), 7.05 (d, 1H), 3.81 (s, 1H), 2.87 (d, 2H), 1.59-1.53 (m, 1H), 1.47-1.34 (m, 4H), 1.25 (s, 4H), 0.88-0.84 (m, 6H). <sup>13</sup>C NMR (101 MHz, CDCl<sub>3</sub>) δ 174.84, 160.94, 155.21, 140.71, 137.94, 136.52, 136.50, 135.85, 135.82, 134.24, 134.22, 128.14, 127.67, 127.40, 125.46, 123.94, 123.92, 72.52, 72.51, 38.89, 37.50, 32.39, 31.59, 28.73, 25.62, 22.93, 14.07, 10.75.

**2b:** 7.66 g, yield: 63%. <sup>1</sup>H NMR (400 MHz, CDCl<sub>3</sub>) δ (ppm): 7.60 (d, 1H), 7.38 (d, 1H), 7.30 (d, 1H), 7.23-7.18 (m, 2H), 7.06 (d, 1H), 7.00 (d, 1H), 3.66 (s, 1H), 2.86 (d, 2H), 1.57-1.51 (m, 1H), 1.48-1.35 (m, 4H), 1.25 (s, 4H), 0.86-0.84 (m, 6H). <sup>13</sup>C NMR (101 MHz, CDCl<sub>3</sub>) δ 174.57, 162.01, 159.97, 159.57, 154.40, 143.56, 143.49, 136.71, 136.02, 134.40, 130.69, 130.66, 127.64, 127.48, 124.74, 124.56, 124.08, 121.14, 121.11, 112.49, 112.25, 72.15, 72.13, 39.00, 37.17, 37.15, 32.29, 28.70, 25.52, 22.89, 14.06, 10.70.

### ***Synthesis of compound 3a and 3b***

To a solution of 3-chloro-2-(2-ethylhexyl)-thiophene (2.37 g, 10.17 mmol) in THF (60 mL) was added *n*-BuLi in hexane (5.5 mL, 8.814 mmol, 1.6 M) slowly at -78 °C under argon protection, and the mixture was stirred at -78 °C for 3 h. Then compound 2a (or 3a) (3 g, 6.78 mmol) was added in one portion and again stirred for 3 h at -78 °C, then followed by slowly warming up to room temperature for 12 h. Subsequently, the mixture was cooled down to room temperature and Tin (II) chloride dihydrate (12.24 g, 54.2 mmol) in 10% HCl (15 mL) was added and then the resulting solution was stirred for an additional 3 h at 50 °C. The reaction was poured into water and then extracted three times with dichloromethane. The organic layer was washed with water, and then dried over anhydrous sodium sulfate. After removal of the solvent, the crude product was purified by column chromatography over silica gel (eluent: petroleum

ether) to give compound 3a (or 3b) as light yellow oil.

**3a:** 2.1 g, yield: 48%. <sup>1</sup>H NMR (400 MHz, CDCl<sub>3</sub>) δ (ppm): 7.63-7.58 (m, 3H), 7.49-7.42 (m, 4H), 7.31 (d, 1H), 7.24 (s, 1H), 3.03 (d, 2H), 2.85 (d, 2H), 1.71-1.66 (m, 2H), 1.53 (d, 2H), 1.45-1.23 (m, 14H), 0.98-0.92 (m, 12H). <sup>13</sup>C NMR (101 MHz, CDCl<sub>3</sub>) δ 138.97, 138.45, 138.23, 138.07, 136.51, 136.25, 136.17, 135.90, 130.84, 129.70, 128.36, 127.98, 127.82, 127.41, 122.97, 122.93, 122.64, 122.36, 40.93, 39.00, 37.59, 32.53, 32.50, 32.07, 28.82, 25.84, 25.73, 23.01, 22.99, 14.12, 10.88, 10.82.

**3b:** 1.9 g, yield: 44%. <sup>1</sup>H NMR (400 MHz, CDCl<sub>3</sub>) δ (ppm): 7.64 (d, 1H), 7.5-7.37 (m, 5H), 7.31 (d, 1H), 7.24 (s, 1H), 3.02 (d, 2H), 2.85 (d, 2H), 1.76-1.64 (m, 2H), 1.54-1.50 (m, 2H), 1.47-1.32 (m, 14H), 0.98-0.90 (m, 12H). <sup>13</sup>C NMR (101 MHz, CDCl<sub>3</sub>) δ 162.15, 159.71, 139.00, 138.30, 138.22, 138.09, 136.52, 136.04, 136.01, 130.81, 130.78, 129.45, 127.98, 127.91, 125.42, 125.39, 125.28, 125.11, 123.05, 122.84, 122.70, 122.60, 116.51, 116.28, 40.92, 39.07, 38.76, 37.21, 37.19, 33.57, 32.51, 32.40, 32.06, 31.61, 29.45, 29.08, 28.82, 28.79, 26.93, 26.21, 25.81, 25.63, 25.46, 23.03, 22.98, 22.83, 22.68, 14.16, 14.15, 10.89, 10.80, 8.38.

#### ***Synthesis of compound 4a and 4b***

To a solution of compound 3a (or 3b) (2.0 g, 3.12 mmol) in THF (60 mL) was added *n*-BuLi in hexane (6.84 mL, 10.95 mmol, 1.6 M) slowly at -78 °C under argon protection, and the mixture was stirred at -78 °C for 3 h. Then trimethyltin chloride in THF (12.5 mL, 12.5 mmol, 1 M) was added in one portion and again stirred for 1h at -78 °C, then slowly warmed up to room temperature for 5 h. The solution was poured into cold deionized water and extracted with diethyl ether three times. The combined organic layer was washed with deionized water three times and dried over anhydrous sodium sulfate. After removal of the solvent, the crude product was recrystallized from ethanol twice to afford compound 4a (or 4b) as yellow solid.

**4a:** 2.2 g, yield: 73%. <sup>1</sup>H NMR (400 MHz, CDCl<sub>3</sub>) δ (ppm): 7.69-7.48 (m, 5H), 7.36-7.29 (m, 1H), 7.25 (s, 1H), 3.05 (d, 2H), 2.90-2.80 (m, 2H), 1.77-1.69 (m, 2H), 1.54-1.33 (d, 16H), 0.99-0.90 (m, 12H), 0.55-0.22 (m, 18H). <sup>13</sup>C NMR (101 MHz, CDCl<sub>3</sub>) δ 143.26, 143.03, 142.56, 142.38, 138.05, 137.71, 137.34, 137.01, 136.98, 136.59, 130.58, 129.82, 129.21, 128.26, 127.58, 122.47, 120.68, 40.87, 39.03, 37.55,

32.55, 32.52, 32.13, 28.86, 28.83, 25.93, 25.76, 23.04, 22.99, 14.16, 14.13, 10.94, 10.84, -6.58, -8.31, -8.34, -10.19.

**4b:** 1.9 g, yield: 70%. <sup>1</sup>H NMR (400 MHz, CDCl<sub>3</sub>) δ (ppm): 7.69-7.62 (s, 1H), 7.54-7.39 (m, 3H), 7.35-7.28 (m, 1H), 7.26 (s, 1H), 3.02 (d, 2H), 2.87-2.84 (dd, 2H), 1.77-1.65 (m, 2H), 1.55-1.45 (m, 4H), 1.44-1.25 (m, 12H), 0.99-0.90 (m, 12H), 0.56-0.23 (m, 18H). <sup>13</sup>C NMR (101 MHz, CDCl<sub>3</sub>) δ 162.16, 159.72, 143.30, 143.13, 143.04, 142.42, 139.06, 138.98, 137.86, 137.35, 136.81, 130.76, 130.61, 130.16, 127.82, 127.67, 125.54, 124.84, 124.66, 122.53, 121.12, 116.61, 116.38, 40.87, 39.12, 37.22, 37.20, 32.54, 32.42, 32.13, 29.72, 28.85, 28.81, 25.92, 25.66, 23.05, 22.97, 14.18, 14.14, 10.94, 10.82.

### ***Synthesis of compound 5a and 5b***

Compound 4a (or 4b) (200 mg, 0.207 mmol), compound 1 (326 mg, 0.621 mmol) and Pd(PPh<sub>3</sub>)<sub>4</sub> (15 mg) were added in a flask under argon protection. Then toluene (30 mL) was injected and the mixture was stirred at 110 °C for 12 h. Then the mixture was quenched with cold deionized water and extracted with chloroform three times. The combined organic layer was washed with deionized water three times and dried over anhydrous sodium sulfate. After removal of the solvent, the crude product was purified by column chromatography over silica gel (eluent: petroleum ether: dichloromethane) to give compound 5a (or 5b) as red solid.

**5a:** 183 mg, yield: 58%. <sup>1</sup>H NMR (400 MHz, CDCl<sub>3</sub>) δ (ppm): 9.87 (s, 2H), 7.69 (d, 2H), 7.62-7.50 (m, 5H), 7.26 (s, 2H), 7.21 (d, 2H), 7.07 (d, 2H), 6.99 (d, 2H), 3.08 (d, 2H), 2.91-2.87 (d, 2H), 2.82-2.78 (m, 4H), 2.75-2.71 (m, 4H), 1.67 (d, 8H), 1.51 (d, 4H), 1.41-1.34 (m, 36H), 1.02-0.90 (m, 26H). <sup>13</sup>C NMR (101 MHz, CDCl<sub>3</sub>) δ 182.52, 146.02, 142.55, 142.22, 141.14, 138.97, 138.69, 138.37, 137.96, 137.88, 137.47, 137.34, 136.98, 136.82, 135.90, 135.82, 135.29, 135.22, 130.61, 130.50, 130.09, 129.58, 129.54, 129.08, 129.03, 128.43, 128.19, 127.86, 125.85, 122.81, 121.60, 118.48, 40.89, 39.01, 37.38, 32.55, 32.22, 31.65, 30.34, 30.22, 29.80, 29.68, 29.29, 29.27, 28.85, 25.96, 25.81, 23.08, 23.02, 22.61, 14.21, 14.15, 14.10, 14.08, 10.95, 10.87.

**5b:** 192 mg, yield: 61%. <sup>1</sup>H NMR (400 MHz, CDCl<sub>3</sub>) δ (ppm): 9.79 (s, 2H), 7.61

(s, 2H), 7.47 (s, 2H), 7.35-7.30 (t, 2H), 7.19-7.13 (m, 4H), 6.99 (d, 4H), 3.67-3.62 (q, 2H), 3.00 (d, 2H), 2.83-2.80 (m, 2H), 2.69 (d, 7H), 1.62-1.50 (m, 10H), 1.44-1.21 (m, 34H), 1.19-1.15 (m, 6H), 0.95-0.83 (m, 24H). <sup>13</sup>C NMR (101 MHz, CDCl<sub>3</sub>) δ 182.50, 145.99, 142.56, 142.26, 141.20, 139.57, 138.73, 138.04, 137.31, 136.78, 135.84, 135.19, 135.08, 130.78, 129.64, 129.15, 128.69, 128.15, 125.89, 122.45, 122.11, 118.49, 37.65, 37.50, 33.47, 31.65, 30.54, 30.37, 30.23, 29.79, 29.70, 29.67, 29.64, 29.35, 29.30, 29.26, 28.06, 26.78, 26.76, 26.45, 22.62, 22.60, 14.09, 14.07.

### ***Synthesis of compound TB and TB-F***

Compound 5a (or 5b) (120 mg, 0.078 mmol), 3-hexylrhodanine (170 mg, 0.78 mmol), and 0.1 ml piperidine were dissolved in dry CHCl<sub>3</sub> (15 mL) under argon protection. The mixture was stirred at 70 °C for 12 h. Then the mixture was quenched with cold deionized water and extracted with chloroform three times. After removing the solvent, the crude product was purified by column chromatography over silica gel (eluent: petroleum ether: chloroform) to give compound **TB (or TB-F)** as purple solid.

**TB:** 149 mg, yield: 59%. <sup>1</sup>H NMR (400 MHz, CDCl<sub>3</sub>) δ (ppm): 7.73 (s, 2H), 7.58-7.50 (m, 4H), 7.42 (s, 1H), 7.26 (s, 2H), 7.12-7.09 (m, 3H), 6.94 (s, 2H), 6.88 (s, 2H), 4.10-4.02 (m, 4H), 3.12 (d, 2H), 2.97-2.87 (m, 2H), 2.75-2.71 (m, 4H), 2.68-2.64 (m, 4H), 1.82-1.60 (m, 14H), 1.53-1.25 (m, 50H), 1.05-0.88 (m, 32H). <sup>13</sup>C NMR (101 MHz, CDCl<sub>3</sub>) δ 192.03, 167.38, 144.25, 141.78, 140.76, 138.95, 138.44, 138.15, 137.69, 137.22, 137.15, 136.88, 135.92, 135.52, 135.30, 135.01, 134.94, 134.49, 130.74, 130.62, 129.78, 129.72, 129.67, 129.60, 128.80, 128.25, 128.05, 127.86, 126.21, 124.80, 122.76, 121.35, 120.08, 118.33, 44.83, 40.85, 39.04, 37.36, 32.60, 32.26, 31.74, 31.70, 31.33, 30.22, 29.96, 29.82, 29.40, 29.38, 28.88, 26.91, 26.46, 25.95, 25.85, 23.12, 23.05, 22.71, 22.67, 22.52, 14.25, 14.16, 14.01, 10.97, 10.91.

**TB-F:** 162 mg, yield: 64%. <sup>1</sup>H NMR (400 MHz, CDCl<sub>3</sub>) δ (ppm): 7.64 (s, 2H), 7.48-7.44 (m, 1H), 7.32-7.28 (m, 3H), 7.19-7.16 (m, 2H), 7.01 (d, 3H), 6.86 (d, 2H), 6.80 (d, 2H), 3.97-3.93 (m, 4H), 3.04 (m, 2H), 2.86-2.83 (m, 2H), 2.67-2.63 (m, 4H), 2.60-2.56 (m, 4H), 1.76-1.59 (m, 16H), 1.32-1.18 (m, 49H), 0.98-0.79 (m, 32H). <sup>13</sup>C NMR (101 MHz, CDCl<sub>3</sub>) δ 190.97, 166.33, 158.49, 143.18, 140.74, 139.71, 137.36, 137.25, 136.62, 136.58, 136.56, 136.08, 135.86, 135.63, 134.67, 134.42, 133.77,

133.68, 133.44, 129.83, 129.78, 129.27, 128.73, 128.70, 127.74, 127.33, 126.90, 125.14, 124.86, 124.68, 124.28, 123.74, 121.78, 120.71, 119.05, 117.25, 116.73, 115.04, 43.79, 39.81, 38.09, 35.99, 31.55, 31.49, 31.21, 30.71, 30.67, 30.29, 29.18, 28.95, 28.81, 28.39, 28.37, 27.83, 25.88, 25.44, 24.90, 24.75, 22.09, 21.99, 21.69, 21.64, 21.50, 13.23, 13.16, 13.14, 12.98, 9.94, 9.86.

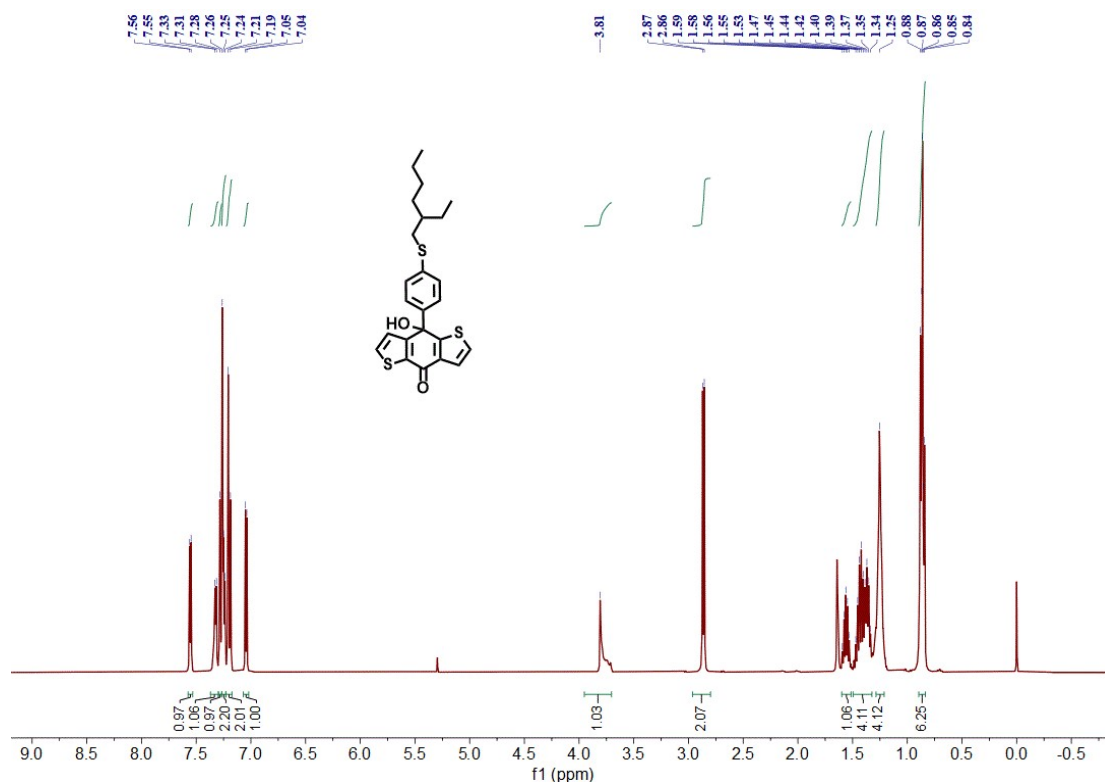


**Figure S1.** <sup>1</sup>H NMR spectrum of compound **2a** in CDCl<sub>3</sub>.

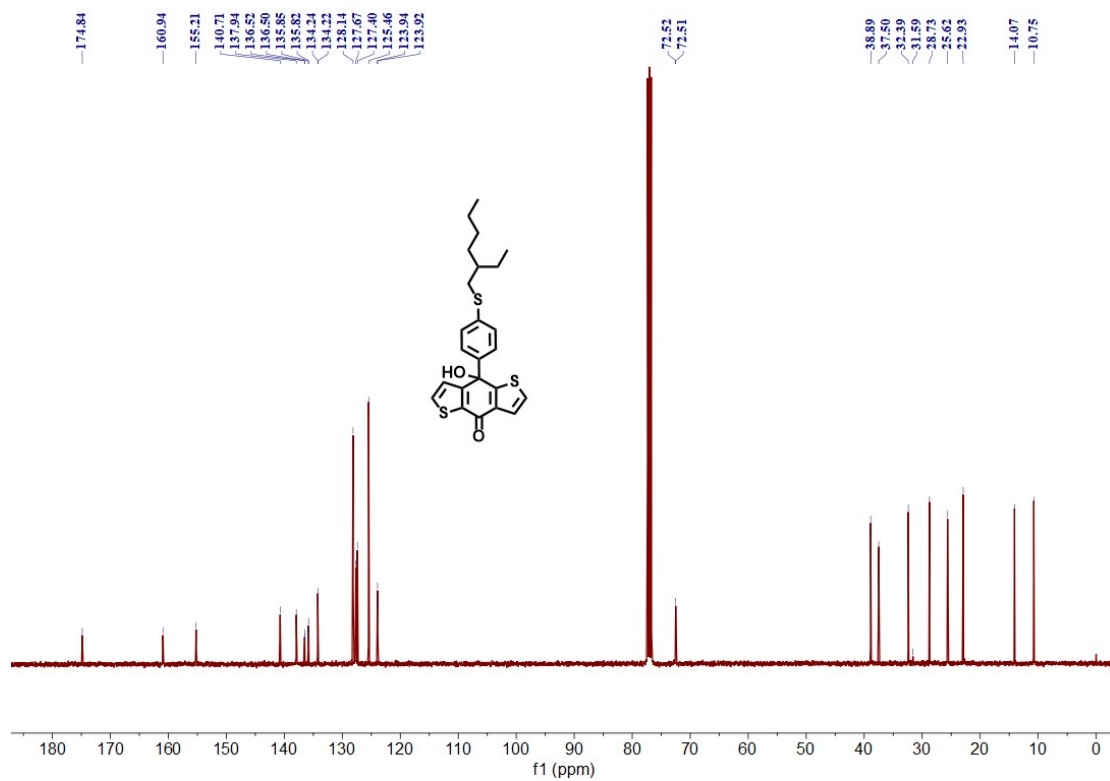


Figure S2.  $^{13}\text{C}$  NMR spectrum of compound **2a** in  $\text{CDCl}_3$ .

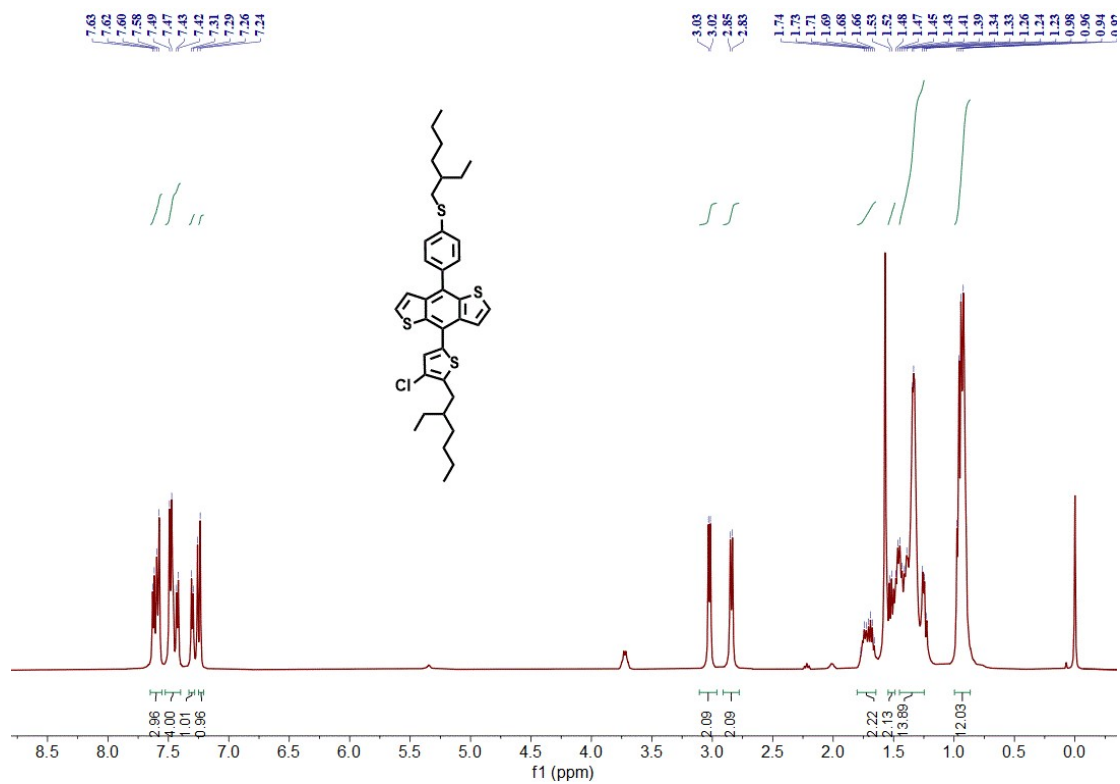
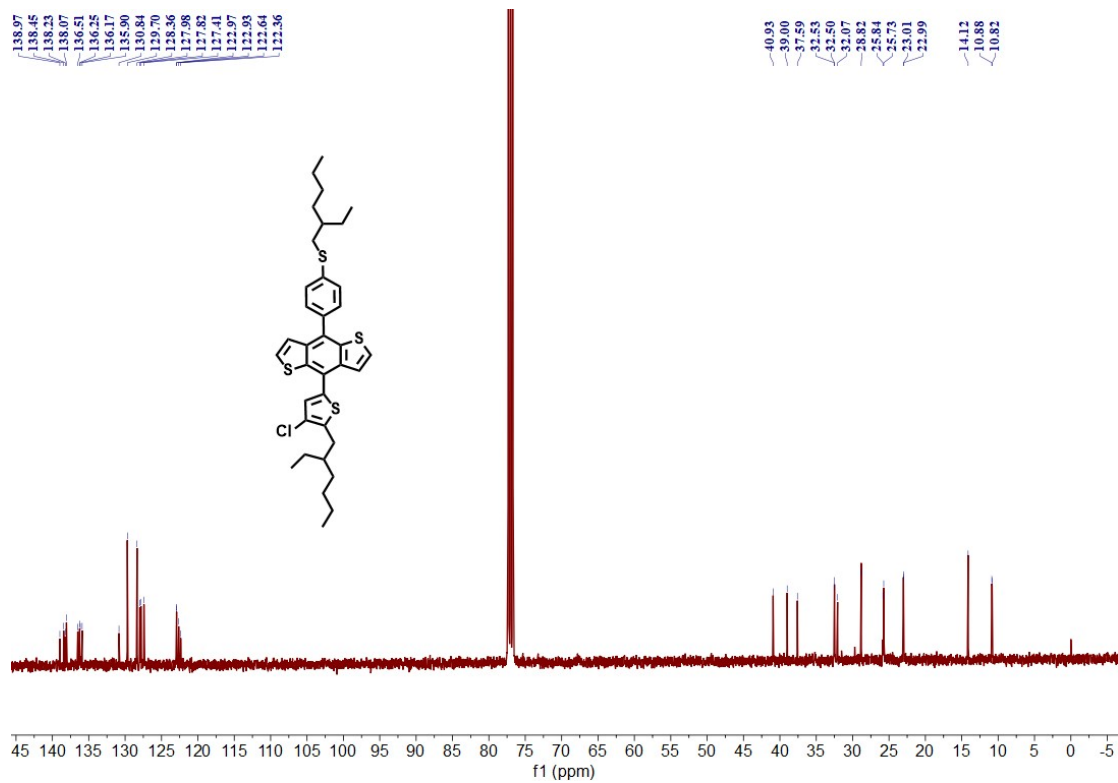
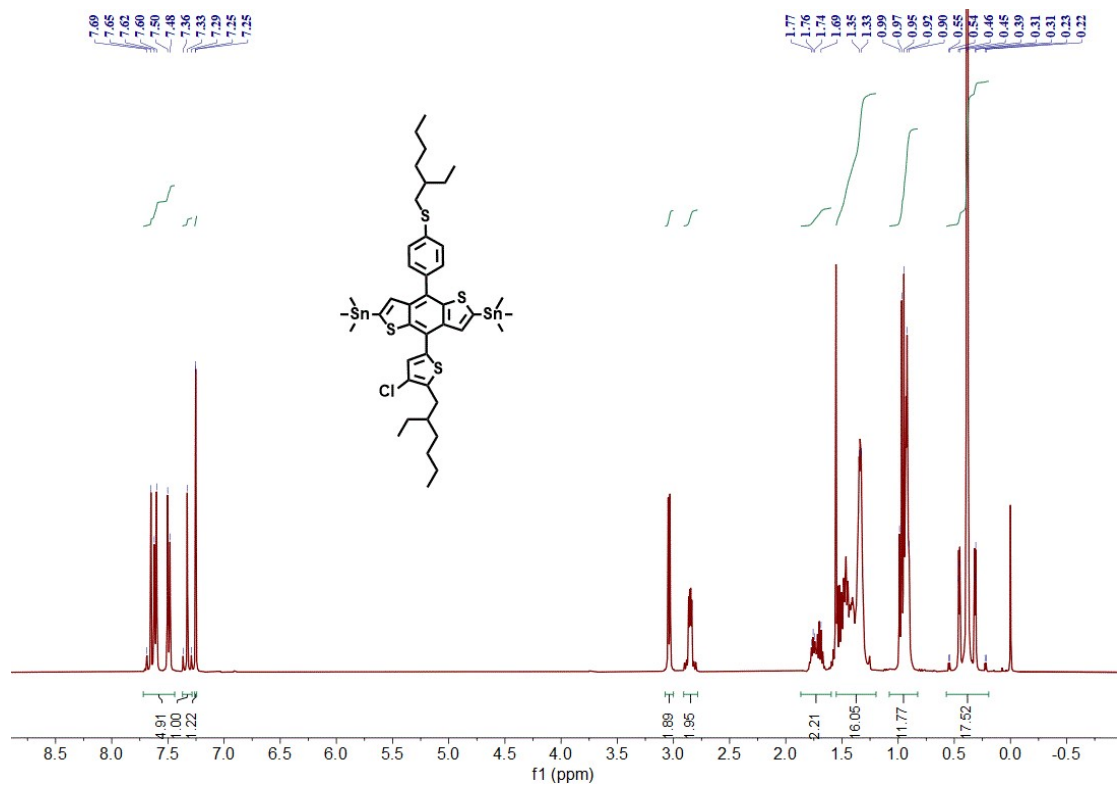


Figure S3.  $^1\text{H}$  NMR spectrum of compound **3a** in  $\text{CDCl}_3$ .



**Figure S4.**  $^{13}\text{C}$  NMR spectrum of compound **3a** in  $\text{CDCl}_3$ .



**Figure S5.**  $^1\text{H}$  NMR spectrum of compound **4a** in  $\text{CDCl}_3$ .

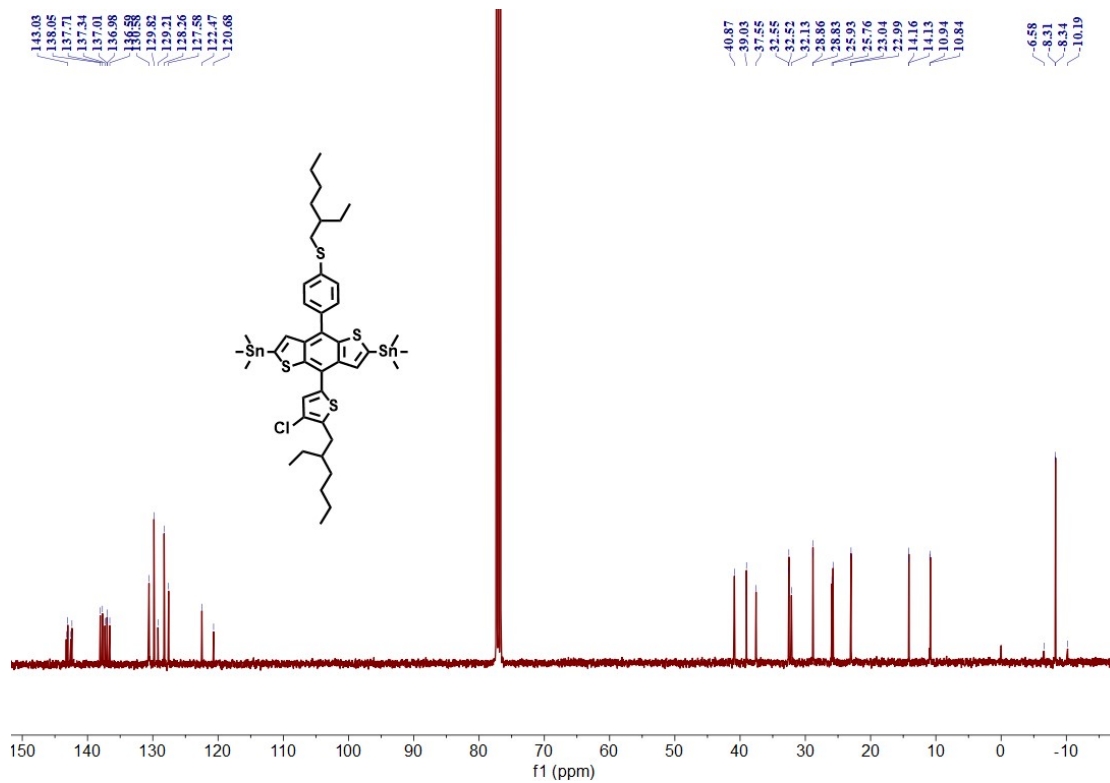


**Figure S6.**  $^{13}\text{C}$  NMR spectrum of compound **4a** in  $\text{CDCl}_3$ .

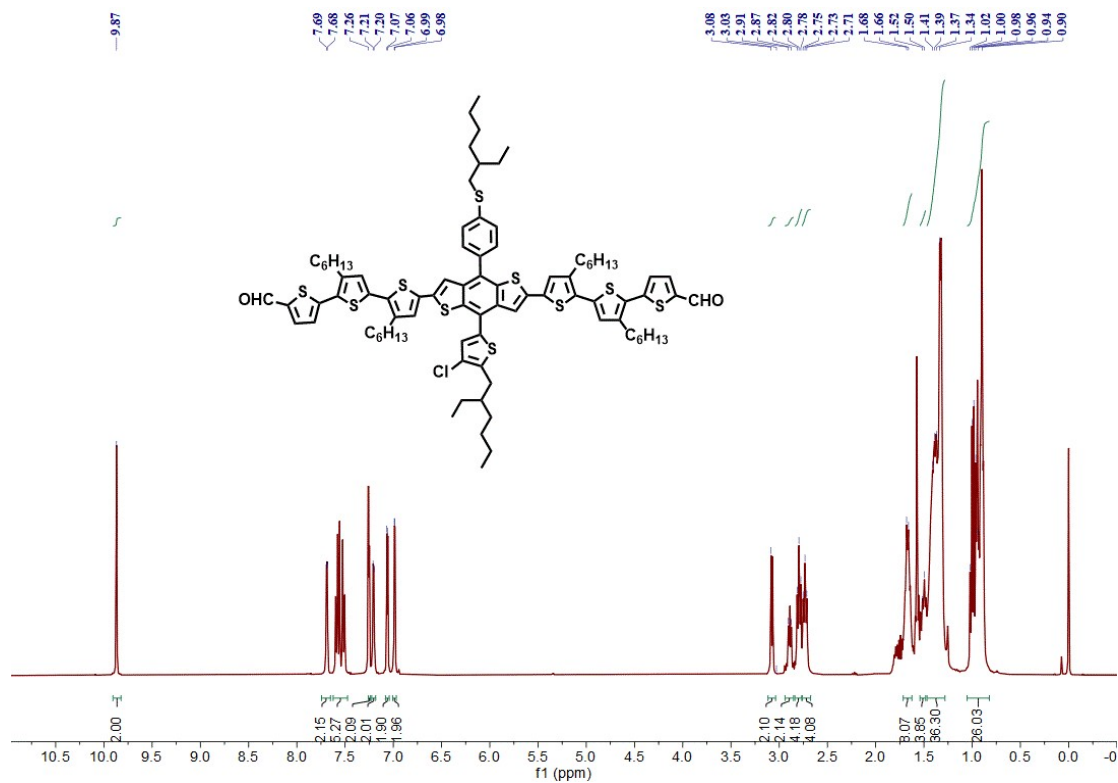


**Figure S7.**  $^1\text{H}$  NMR spectrum of compound **5a** in  $\text{CDCl}_3$ .

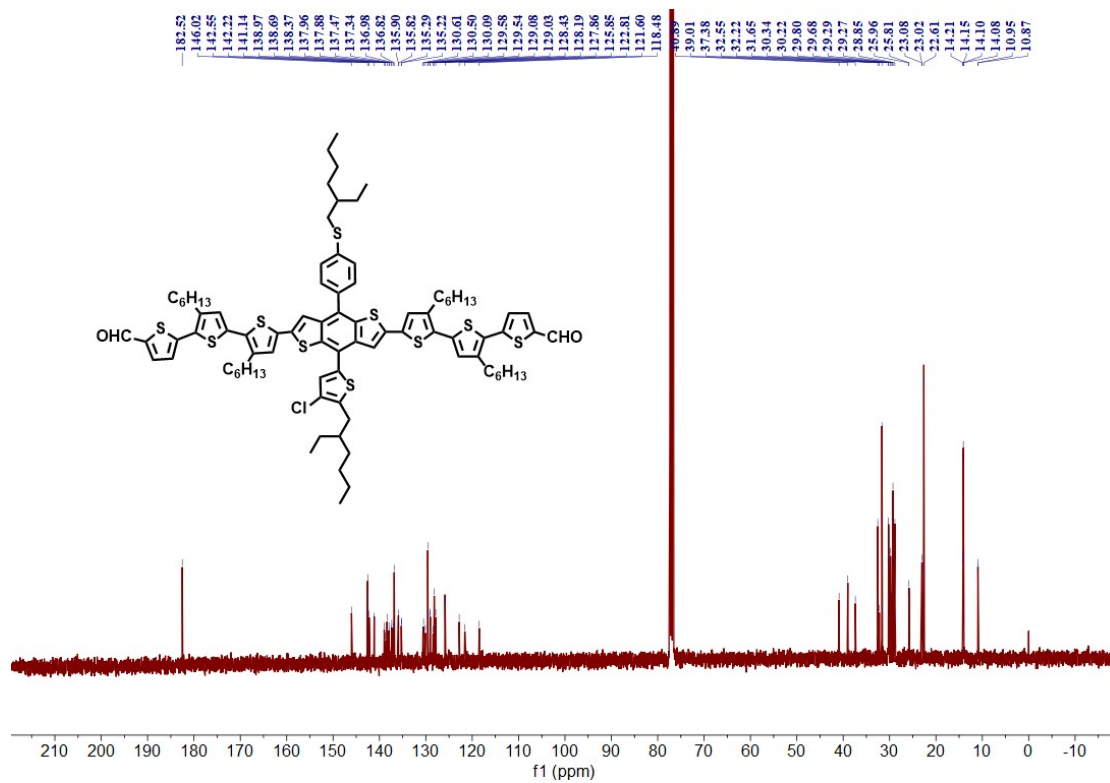


Figure S8.  $^{13}\text{C}$  NMR spectrum of compound **5a** in  $\text{CDCl}_3$ .

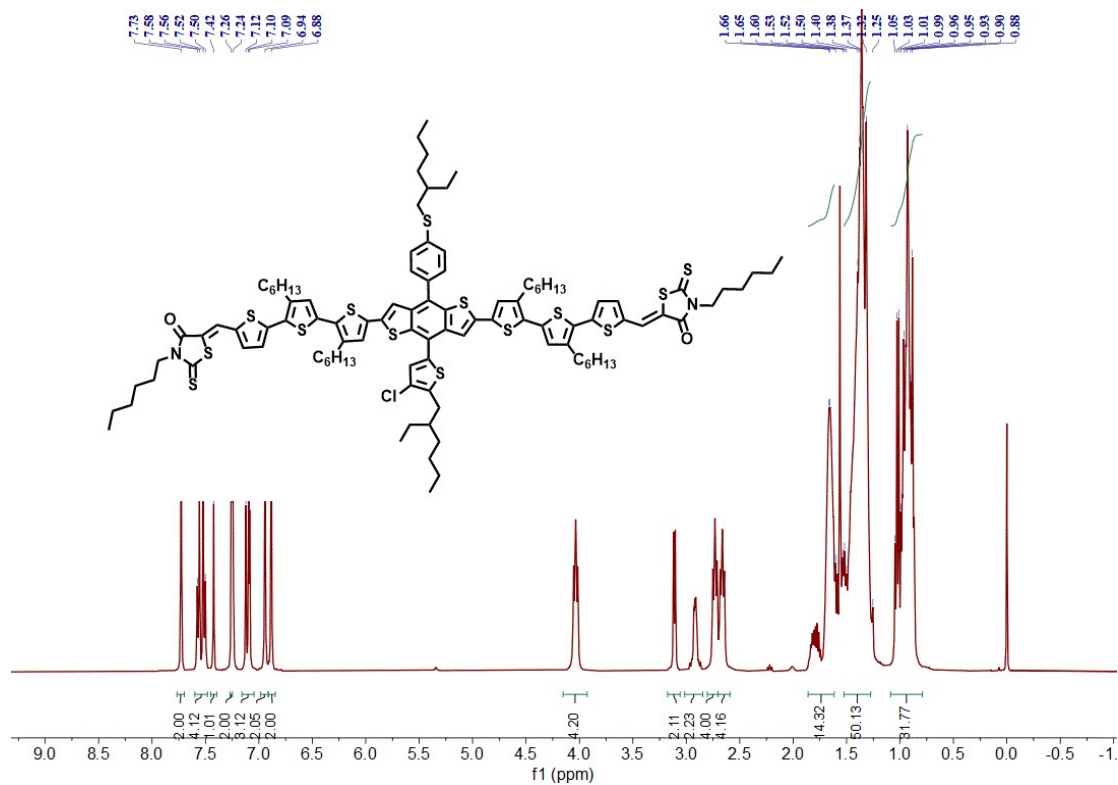


Figure S9.  $^1\text{H}$  NMR spectrum of compound **TB** in  $\text{CDCl}_3$ .

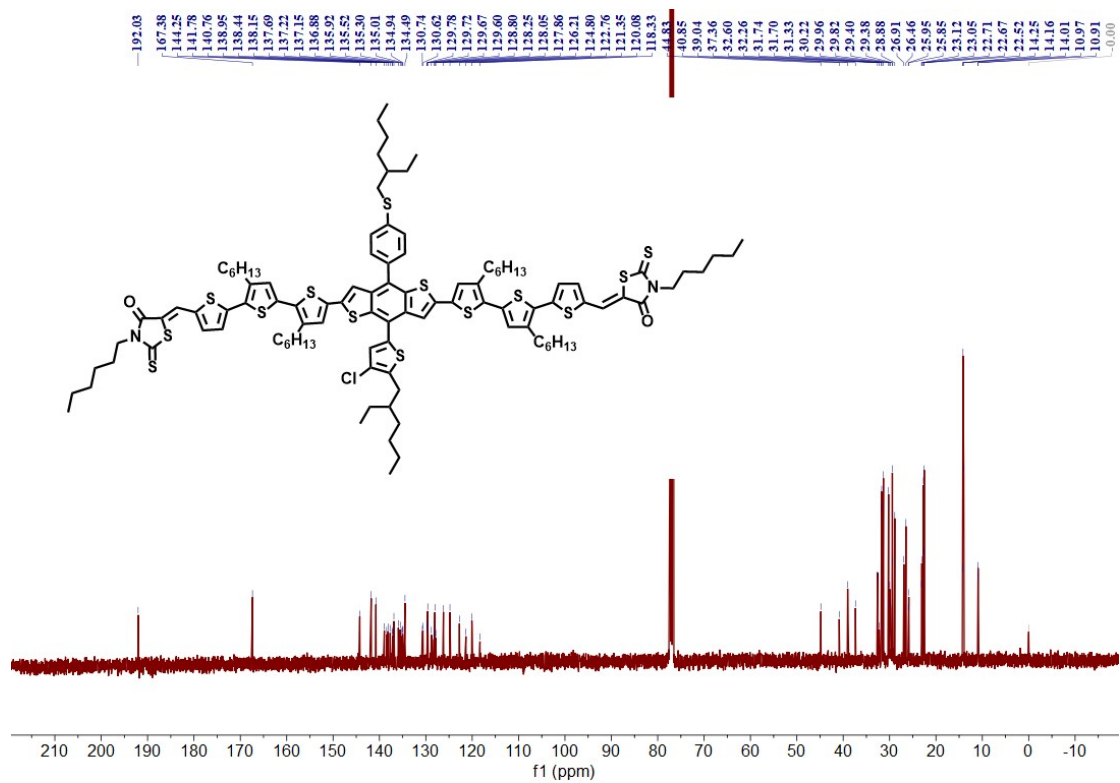


Figure S10.  $^{13}\text{C}$  NMR spectrum of compound TB in  $\text{CDCl}_3$ .

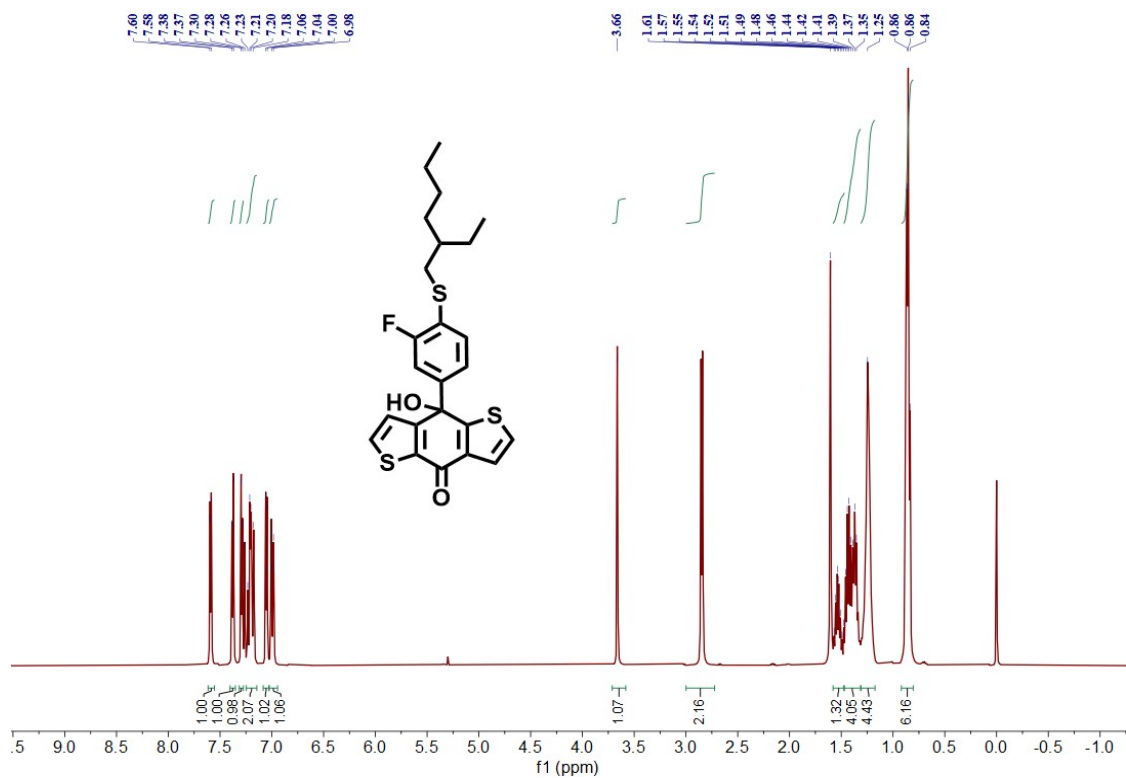


Figure S11.  $^1\text{H}$  NMR spectrum of compound 2b in  $\text{CDCl}_3$ .

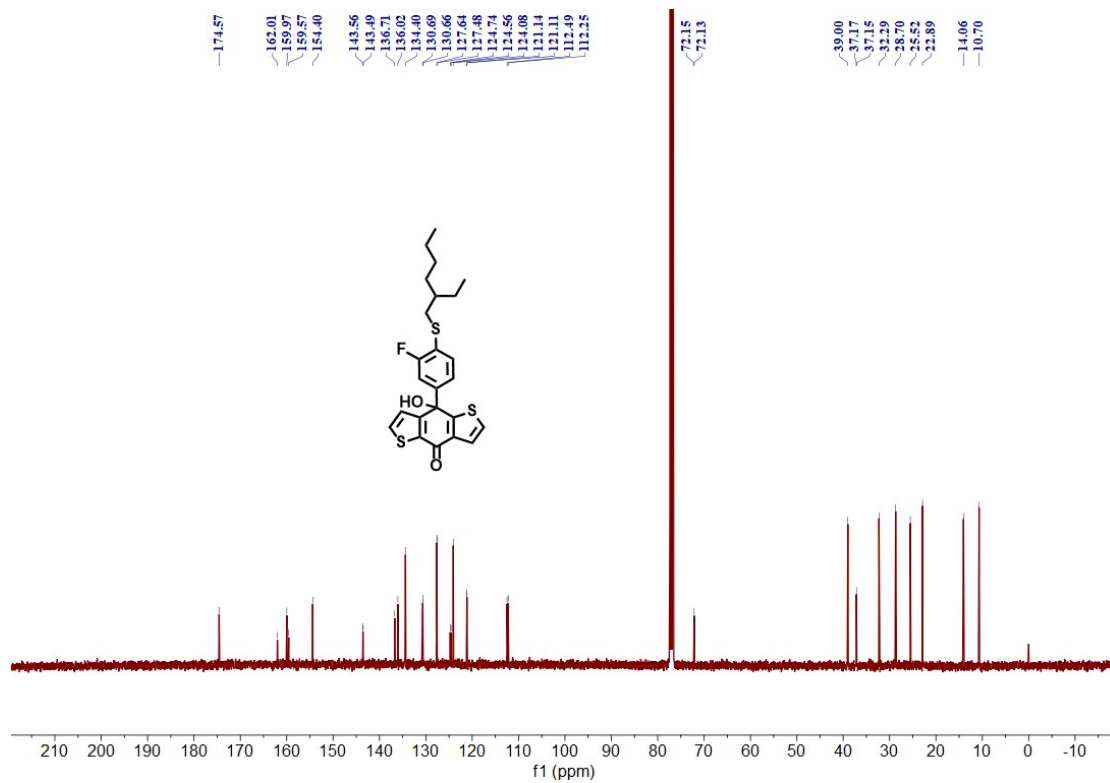


Figure S12.  $^{13}\text{C}$  NMR spectrum of compound **2b** in  $\text{CDCl}_3$ .

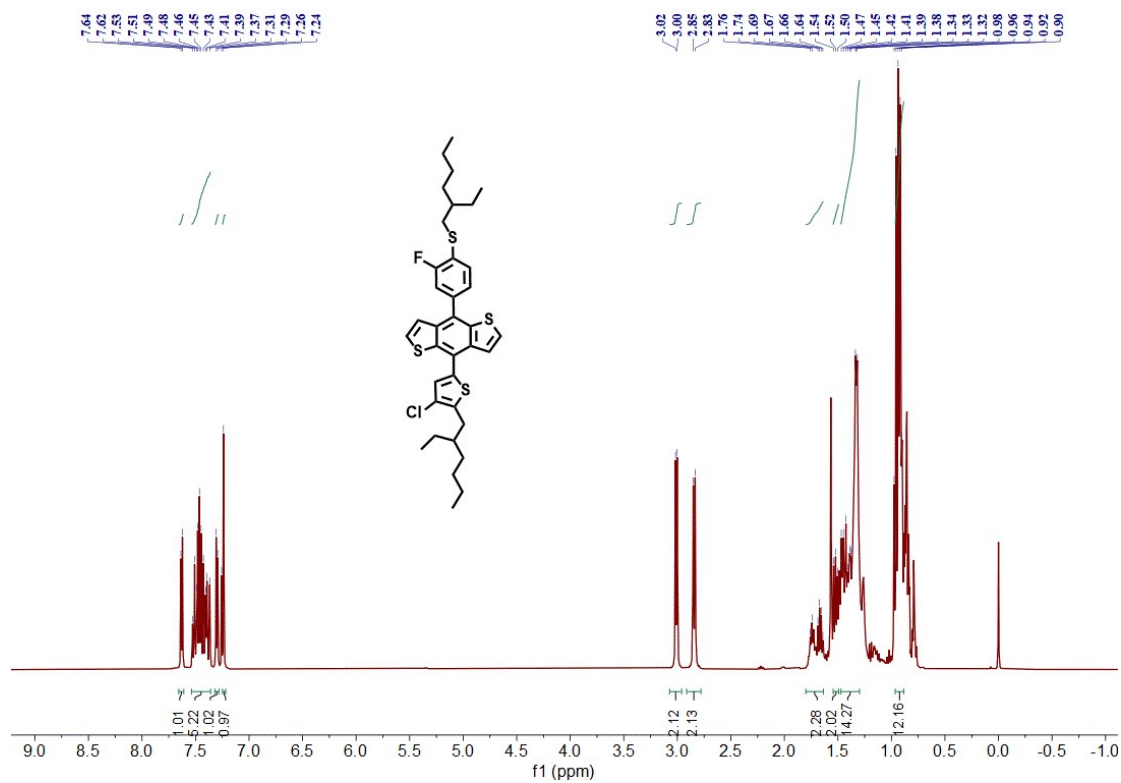
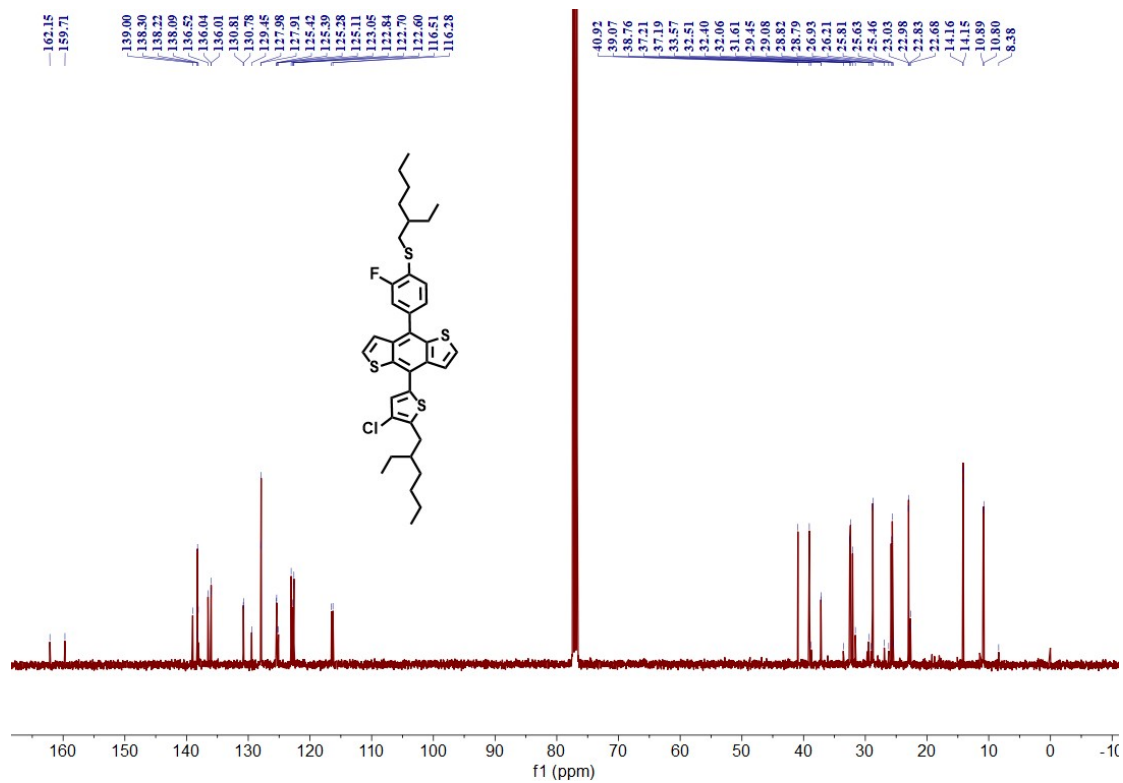
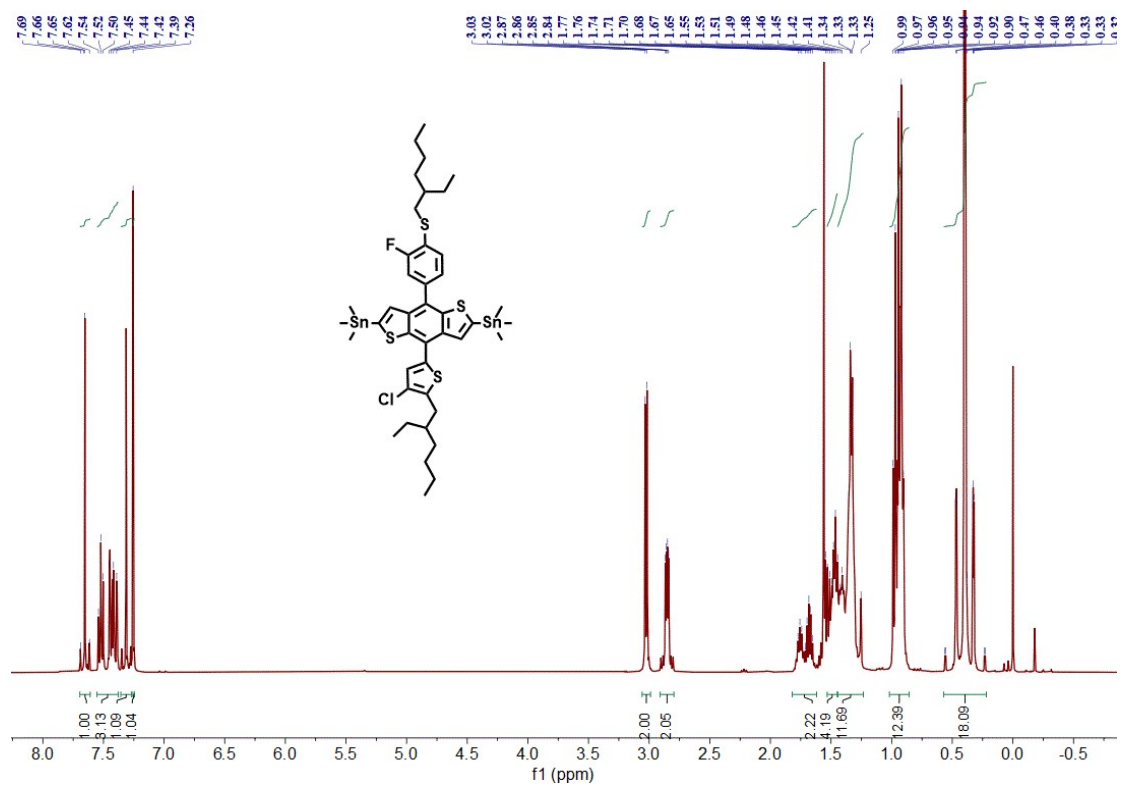


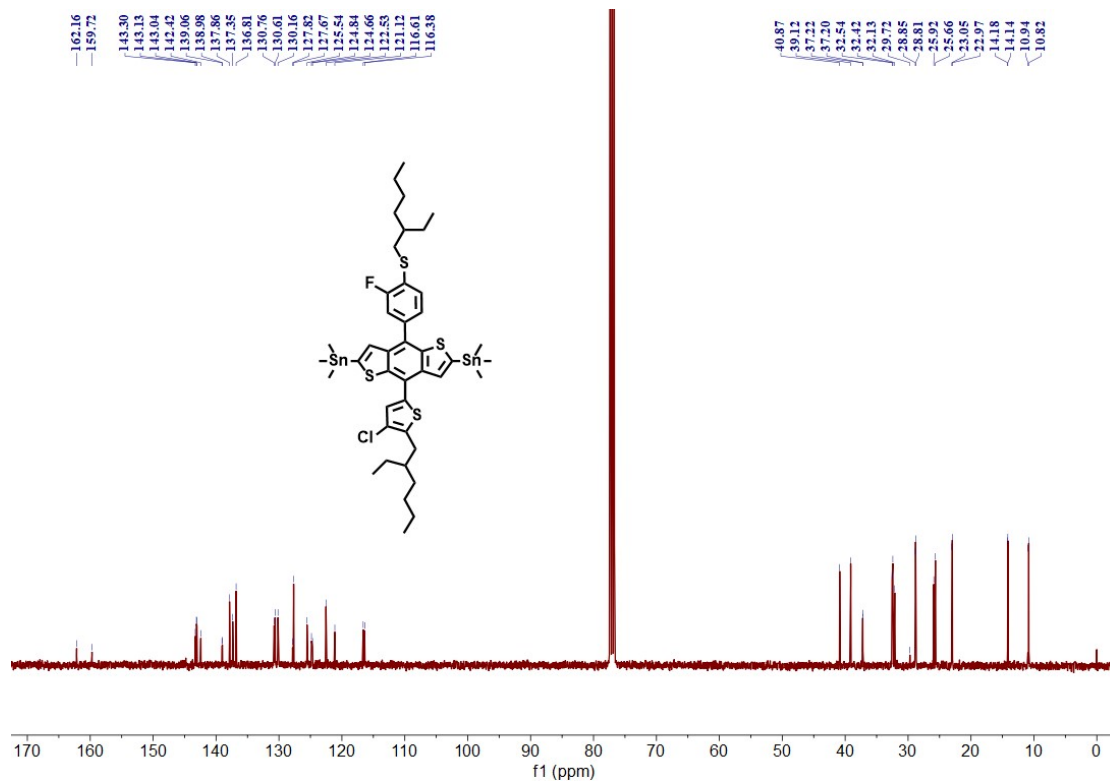
Figure S13.  $^1\text{H}$  NMR spectrum of compound **3b** in  $\text{CDCl}_3$ .



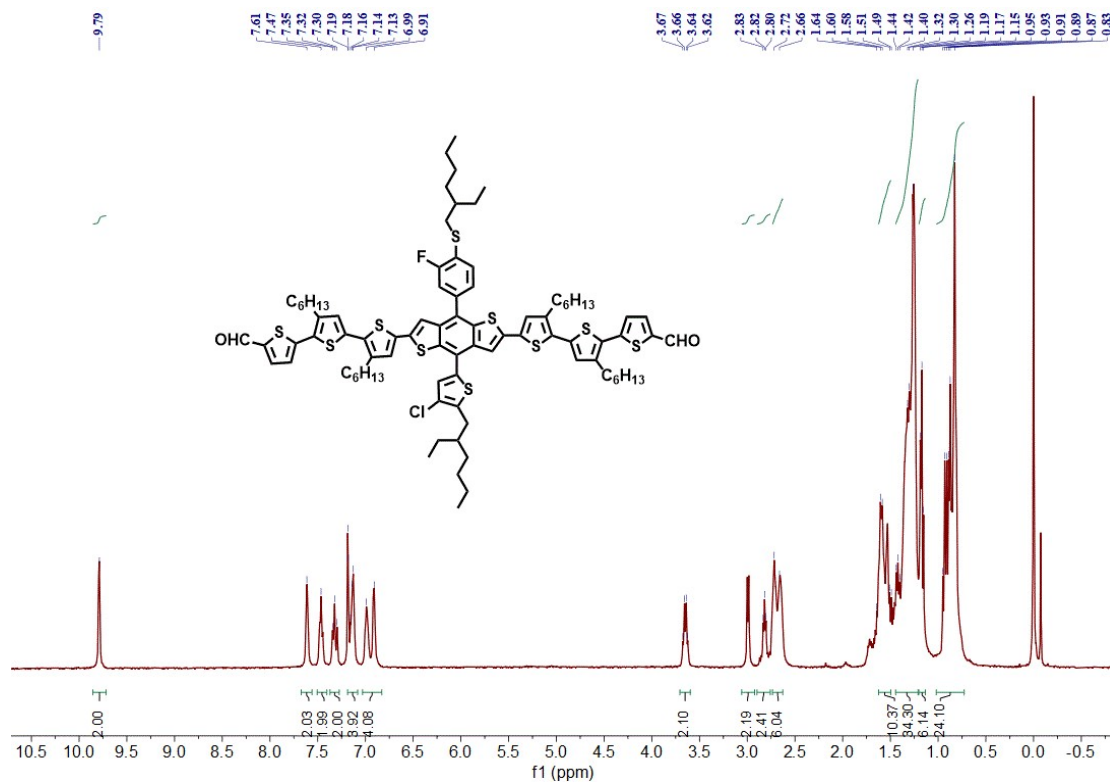
**Figure S14.**  $^{13}\text{C}$  NMR spectrum of compound **3b** in  $\text{CDCl}_3$ .



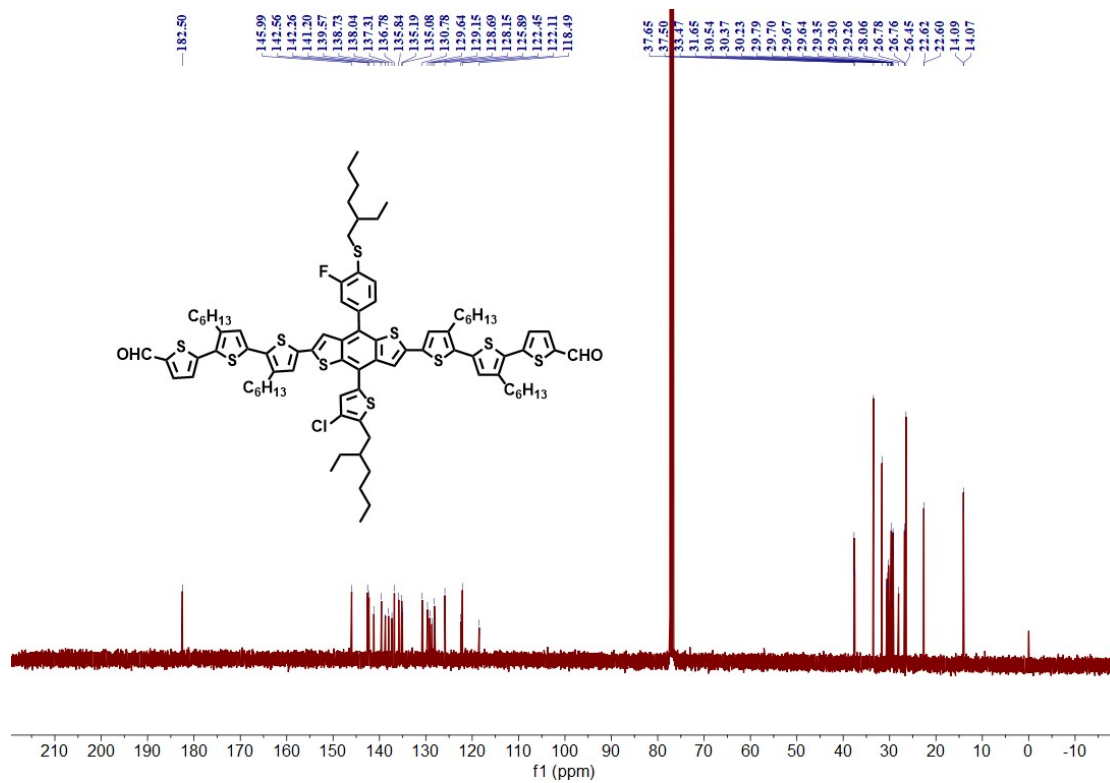
**Figure S15.**  $^1\text{H}$  NMR spectrum of compound **4b** in  $\text{CDCl}_3$ .



**Figure S16.**  $^{13}\text{C}$  NMR spectrum of compound **4b** in  $\text{CDCl}_3$ .



**Figure S17.**  $^1\text{H}$  NMR spectrum of compound **5b** in  $\text{CDCl}_3$ .



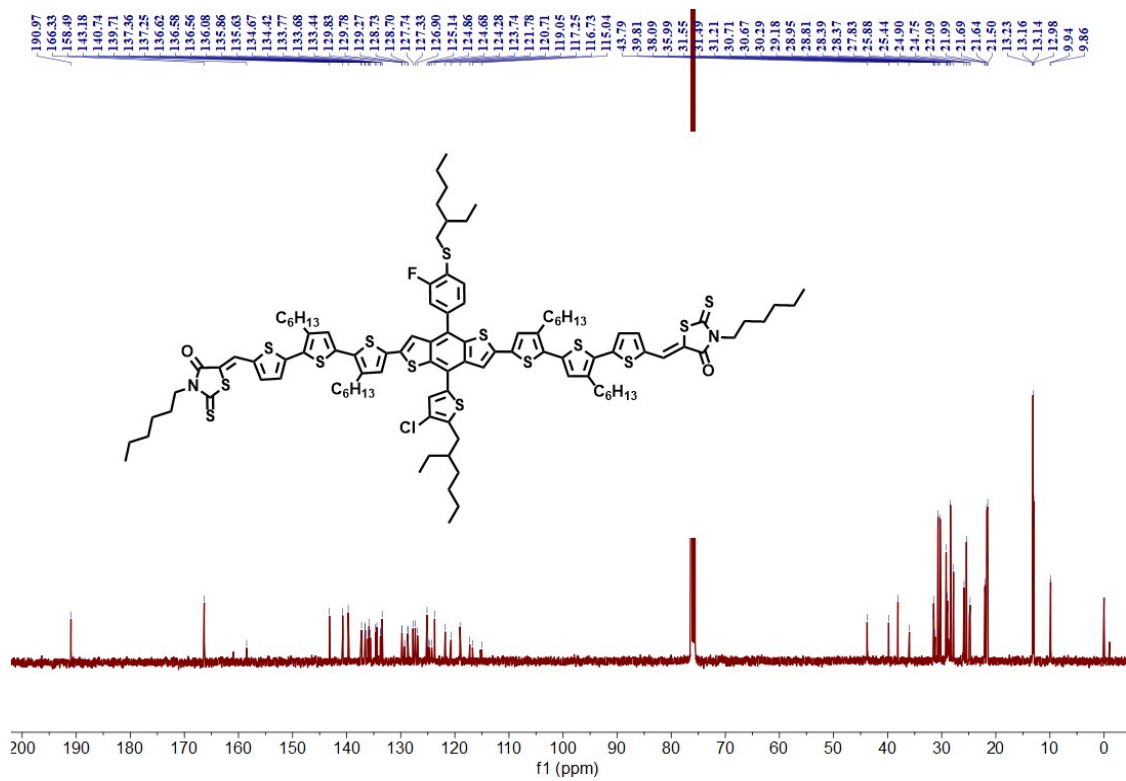


**Figure S20.**  $^{13}\text{C}$  NMR spectrum of compound **TB-F** in  $\text{CDCl}_3$ .

### 3. Reported high-performance ASM-OSCs

**Table S1.** Statistical sheet of PCEs of high performance ASM-OSCs

Time	Donor	Acceptor	$V_{oc}$ [V]	$J_{sc}$ [mA cm <sup>-2</sup> ]	FF (%)	PCE (%)	Ref.
2019	BSFTR	Y6	0.85	23.16	69.66	13.69	[2]
2019	ZR1	Y6	0.86	24.34	68.44	14.34	[3]
2019	BTR-Cl	Y6	0.86	24.17	65.5	13.61	[4]
2020		Y6	0.83	23.66	74.7	14.7	[5]
2019	BTEC-2F	Y6	0.854	21.55	72.35	13.34	[6]
2020	BTTZR	Y6	0.88	23.2	68	13.9	[7]
2020	BT-2F	Y6	0.85	22.38	72.27	13.80	[8]
		N3	0.845	24.28	75.02	15.39	[9]
2020	SM1-F	Y6	0.87	23.25	69.9	14.07	[10]
2020	B1	BO-4Cl	0.83	25.27	73	15.3	[11]
2021		BTP-eC9	0.832	24.98	75.44	15.68	[12]
2020	TBFT-TR	Y6	0.784	24.59	72.78	14.03	[13]
2020	TBD-S4	Y6	0.854	24.53	72.1	15.1	[14]
2021	TBD-S2	Y6	0.85	22.3	69.1	13.1	[15]
2020	ZR2-C3	Y6	0.854	24.69	70.06	14.78	[16]
2021	SM-BF1	Y6	0.846	26.64	69.7	15.71	[17]
2021	SL1	Y6	0.88	23.2	68	13.9	[18]
2021	BTR-BT	Y6	0.78	24.9	69.9	13.63	[19]
2021	FYSM-SiCl	Y6	0.85	23.7	66.8	13.4	[20]
2021	L2	Y6	0.83	26.35	72.1	15.8	[21]
2021	M-PhS	BTP-eC9	0.84	25.4	75.6	16.2	[22]
2022	C-2F	N3	0.85	24.87	69.33	14.64	[23]
2022	BSFTR	FO-2Cl	0.885	22.01	78.41	15.27	[24]
		Fo-EH-2Cl	0.876	22.39	80.44	15.78	[24]
2022	BTR-SCl	Y6	0.88	23.4	70.8	14.6	[25]
2022	SM-CA-Reh	N3	0.84	25.42	77.50	16.3	[26]
2022	ZR-SiO-EH	Y6	0.87	25.6	73.7	16.4	[27]
2022	TB	L8-Bo	0.86	24.67	74.2	15.8	This work
2022	TB-F	L8-Bo	0.87	25.41	76.7	17.0	This work

## 4. Density Functional Theory Calculation

Theoretical calculations were performed to investigate the geometry and frontier molecular orbitals of the three SMDs by density functional theory (DFT) at the B3LYP/631G(d,p) level. All of the alkyl side chains were replaced with methyl groups to simplify the calculations.

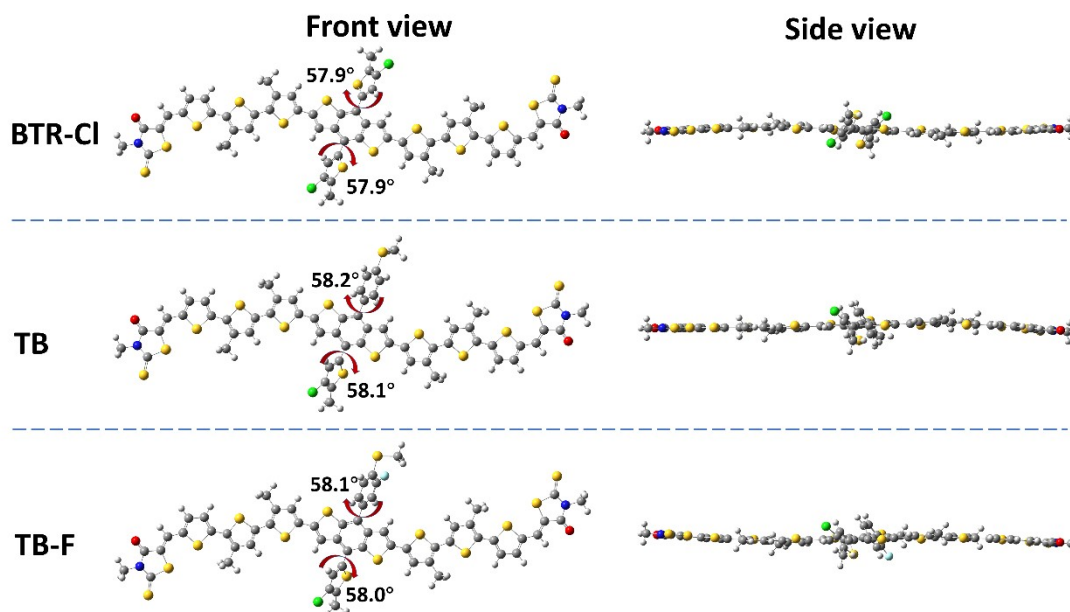


Figure S21. Chemical geometry of the molecular models.

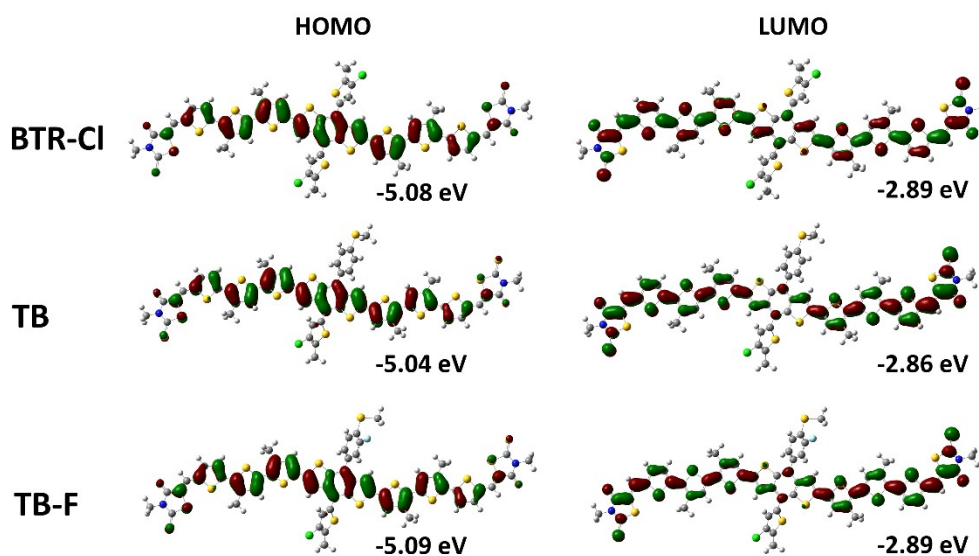
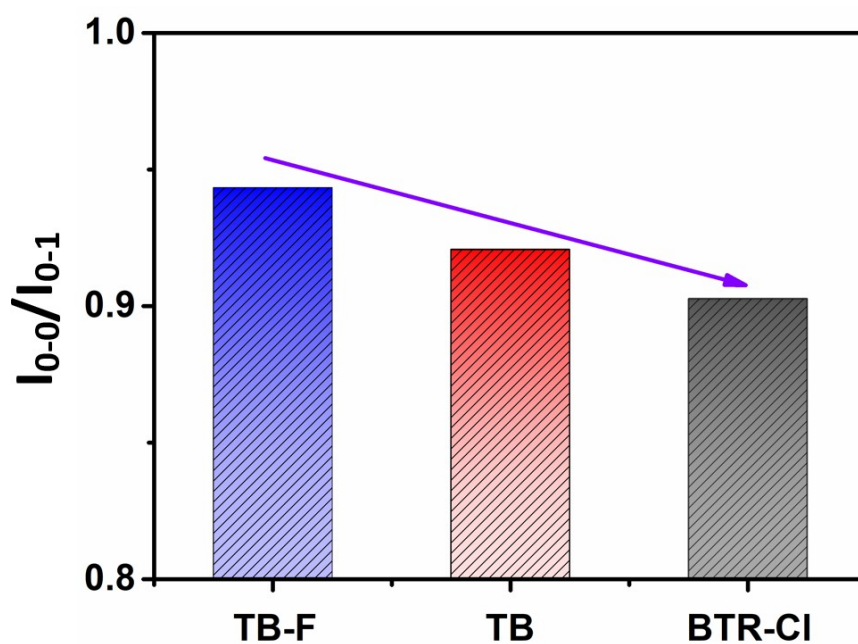


Figure S22. HOMO and LUMO energy levels of the small molecular donors estimated by DFT calculation

## 5. UV-Vis Absorption

The UV-vis absorption spectra of solutions and films were recorded using a Hitachi U-4100 spectrophotometer. The **BTR-Cl**, **TB**, and **TB-F** solutions were prepared at 0.01 mg/mL in chloroform and measured at room temperature. The film optical absorption spectra were recorded from films cast from chloroform solutions (5.0 mg/mL, 1500 rpm) onto quartz plate.



**Figure S23.** Comparison of the intensity value based on 0-0/0-1 absorption peak for three small molecular donors.

## 6. Cyclic Voltammetry

Cyclic voltammetry (CV) measurement was recorded on a CHI660D electrochemical workstation with a three-electrode system (a glassy carbon working electrode, an Ag/Ag<sup>+</sup> electrode as reference electrode and a platinum wire counter electrode) using a scan rate of 100 mV/s with a nitrogen saturated solution of 0.1 M tetrabutylammonium hexafluorophosphate (Bu<sub>4</sub>NPF<sub>6</sub>) in acetonitrile. The BTR-Cl, TB and TB-F materials were drop-cast onto the working electrode from 5 mg/mL CHCl<sub>3</sub> solutions. A ferrocene-ferrocenium (Fc/Fc<sup>+</sup>) redox couple was used as an internal standard and was assigned an absolute energy of -4.8 eV vs vacuum. The HOMO and LUMO energy levels of the materials were determined according to the equation  $E_{\text{HOMO/LUMO}} = -(E_{\text{oxonset}}/E_{\text{redonset}} - E_{\text{Fc/Fc}^+} + 4.80)$ .

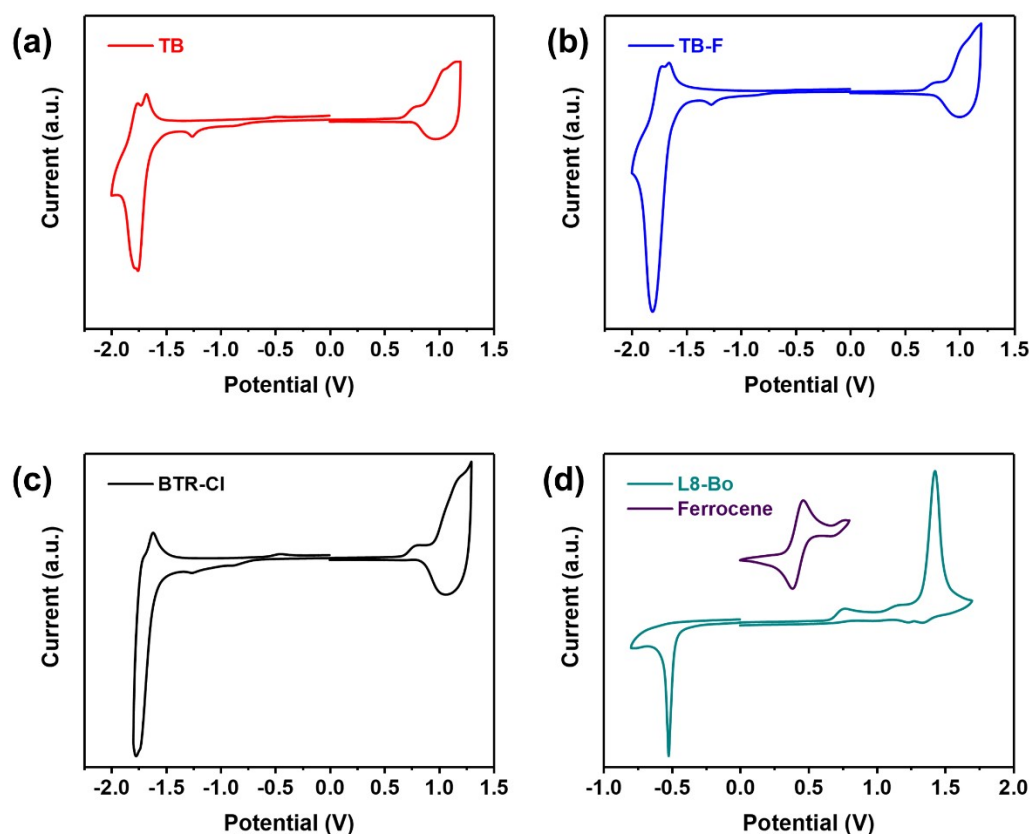


**Figure S24.** Cyclic voltammograms of the small molecular donors and acceptor.

## 7. Ultraviolet Photoelectron Spectroscopy Measurement

BTR-Cl, TB, TB-F and L8-Bo neat films were obtained by spin-coating their solutions onto clean silicon substrates. Silicon substrates were first washed and cleaned with deionized water and isopropanol. Then, neat BTR-Cl, TB, TB-F and L8-Bo films were obtained by spin-coating from 14 mg/mL chloroform solutions.

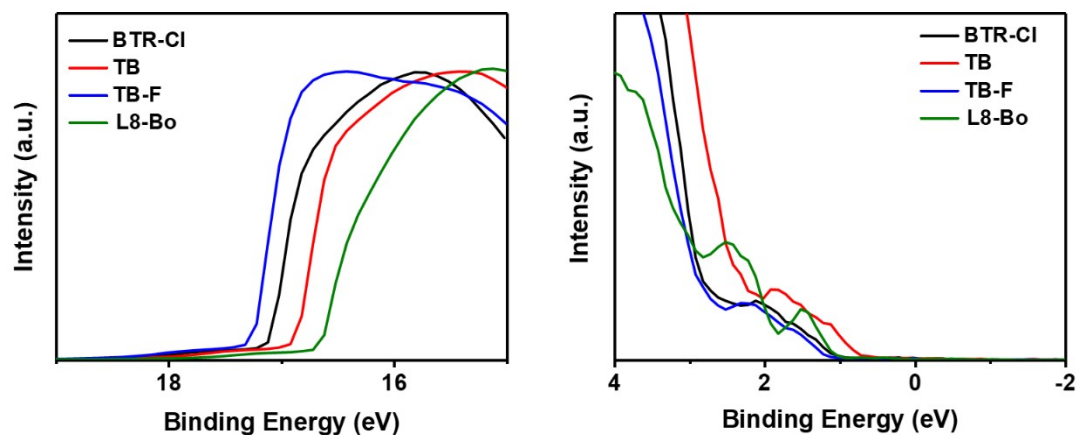


**Figure S25.** Cutoff and valence band regions of the UPS spectra of all the donors and acceptor. Fermi level is set at 0.0 eV.

**Table S2.** UPS-HOMO/LUMO estimated from UPS measurement

Materials	UPS-HOMO (eV)	UPS-LUMO (eV)
BTR-Cl	-5.34	-3.44
TB	-5.29	-3.39
TB-F	-5.34	-3.44
L8-Bo	-5.68	-4.21

## 8. Contact Angle

Contact angles were measured with a contact angle meter (GBX DIGIDROP). The solution of each organic material was spin-coated on cleaned ITO substrates. Droplets of water and glycerol were dripped onto the different films.

According to Owens-Wendt method, surface tension could be divided into dispersive and polar components:  $\gamma = \gamma^d + \gamma^p$

Furthermore, the dispersive and polar surface tension can be calculated through the formula below based on the contact angles obtained by two solvents.

$$(1 + \cos \theta)\gamma_L = 2\sqrt{\gamma_S^d \gamma_L^d} + 2\sqrt{\gamma_S^p \gamma_L^p}$$

where  $\theta$  is the contact angle of a specific solvent,  $\gamma_L$  is the surface tension of the solvent,  $\gamma_S^d$  and  $\gamma_S^p$  refer to the dispersive and polar surface tension of the solid, respectively, and  $\gamma_L^d$  and  $\gamma_L^p$  refer to the dispersive and polar surface tension of the solvent, respectively.

Thus, the unknown values  $\gamma_S^d$  and  $\gamma_S^p$  can be solved through combining two equations obtained by contact angle measurement of two different solvents.

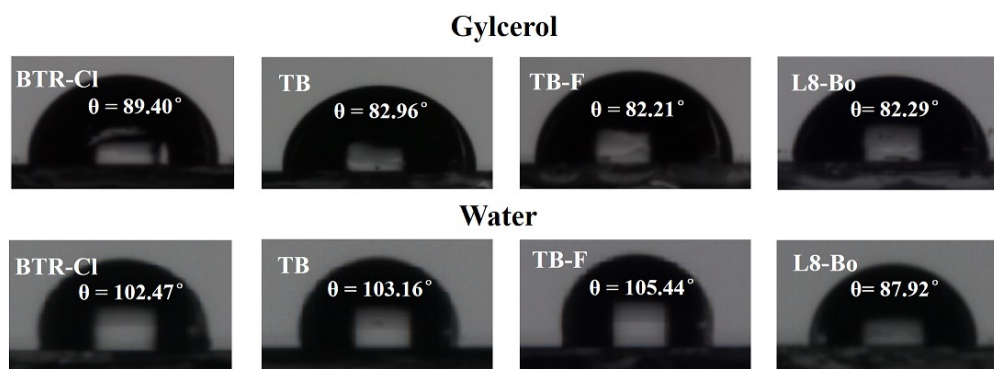


**Figure 26.** Contact angles of the small molecules.

### Calculation of Flory-Huggins interaction parameter ( $\chi$ ) by contact angle

Solubility parameter ( $\delta$ ) can be calculated from the surface tension:

$$\delta = K\sqrt{\gamma}$$

where  $\gamma$  is the surface tension, K is the proportionality constant ( $K = 116 \times 10^3 \text{ m}^{-1/2}$ ).

Flory-Huggins interaction parameter ( $\chi_{ij}$ ) can be written as a function of two solubility

parameter:

$$\chi_{ij} = \frac{V_0}{RT}(\delta_i - \delta_j)^2$$
 where  $\chi_{ij}$  is the Flory–Huggins interaction parameter between the material  $i$  and  $j$ ,  $V_0$  is the geometric mean of the polymer segment molar volume,  $R$  is the gas constant,  $T$  is the absolute temperature, and  $\delta_i$  and  $\delta_j$  are the solubility parameter of material  $i$  and  $j$ , respectively. To simplify, we define the parameter  $\kappa = K^2V_0/RT$ , then the Flory–Huggins interaction parameter can be written as the formula below,  
$$\chi_{ij} = \kappa(\sqrt{\gamma_i} - \sqrt{\gamma_j})^2$$
 where  $\gamma_i$  and  $\gamma_j$  are the surface tension of material  $i$  and  $j$ , respectively.

**Table S3.** Contact angle and surface tension values of the donors and acceptor

Pristine films	$\theta_{\text{GI}} [^\circ]$	$\theta_{\text{water}} [^\circ]$	$\gamma [\text{mN m}^{-1}]$
BTR-Cl	89.40	102.47	11.69
TB	82.96	103.16	14.30
TB-F	82.21	105.44	15.52
L8-Bo	82.29	87.92	20.36

## 9. Grazing Incidence Wide-Angle X-Ray Scattering

2D-GIWAXS experiments were carried out on a GANESHA 300XL+ system from JJ

X-ray. The instrument is equipped with a Pilatus 300K detector, with pixel size of  $172 \times 172 \mu\text{m}$ . The X-ray source is a Genix 3D Microfocus Sealed Tube X-Ray Cu-source with integrated Monochromator (30 W). The wavelength used is  $\lambda = 1.5418 \text{ \AA}$ . The detector moves in a vacuum chamber with sample-to-detector distance varied between 0.115 m and 1.47 m depending on the configuration used, as calibrated using silver behenate ( $d_{001} = 58.380 \text{ \AA}$ ). The minimized background scattering plus high-performance detector allows for a detectable  $q$ -range varying from  $3 \times 10^{-3}$  to  $3 \text{ \AA}^{-1}$  (0.2 to 210 nm). The sample was placed vertically on the goniometer and tilted to a glancing angle of  $0.2^\circ$  with respect to the incoming beam. A small beam was used to get a better resolution. The accumulation time was 30 minutes for each measurement. In-plane and out-of-plane line-cuts were obtained using SAXSGUI program.

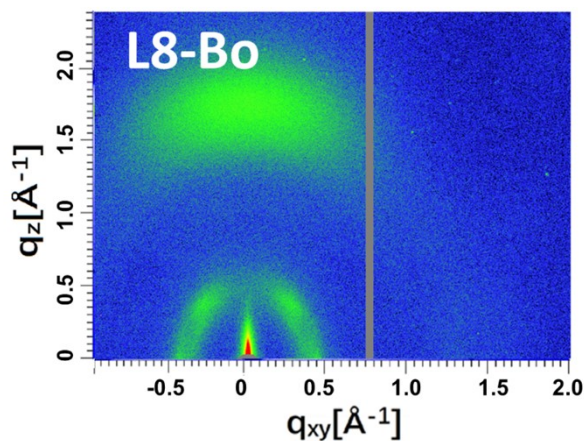


**Figure S27.** 2D-GIWAXS pattern of L8-Bo films.

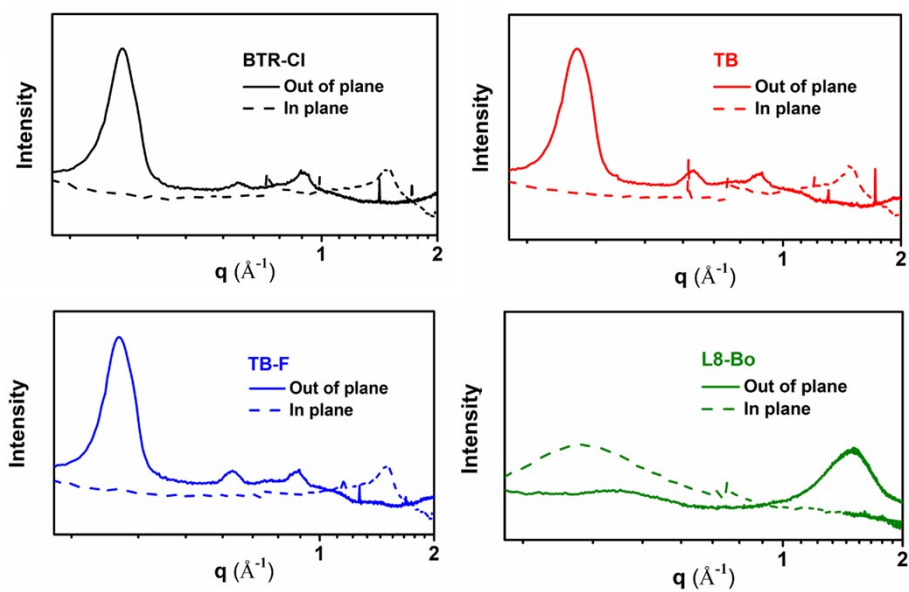


**Figure S28.** 1D-GIWAXS line-cut profiles of the neat BTR-Cl, TB, TB-F and L8-Bo films.

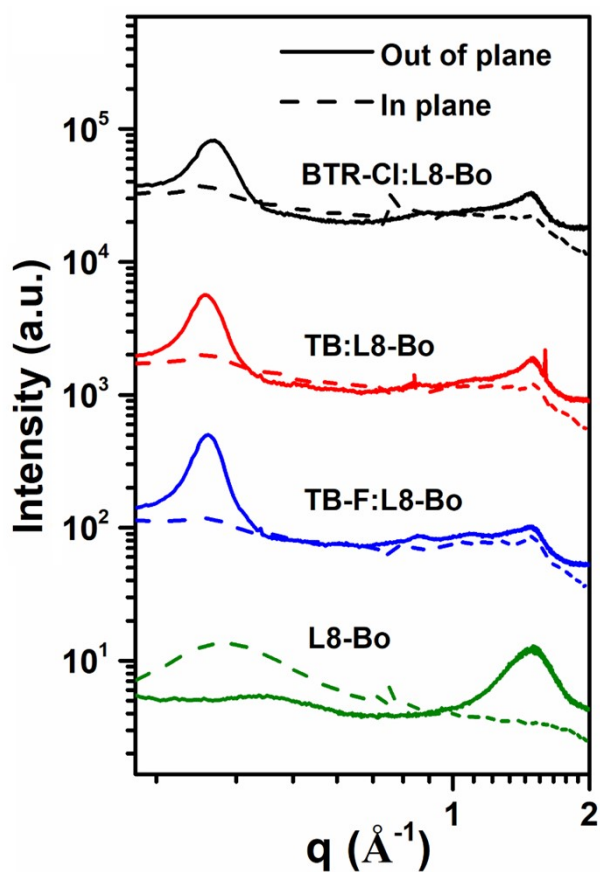


**Figure S29.** 1D-GIWAXS line-cut profiles of the BTR-Cl:L8-Bo, TB:L8-Bo, TB-F:L8-Bo, and L8-Bo films.

## 10. Solar cell device fabrication and characterization

OSC devices were fabricated with a conventional device structure of ITO/PEDOT:PSS/active layer/electron transportation layer (ETL)/Ag. The ITO-coated glass substrates were sonicated successively with detergent, deionized water, acetone and isopropanol, and dried with nitrogen flow. Immediately prior to device fabrication, the substrates were cleaned by oxygen plasma for 5 min. And then, the PEDOT:PSS layer was spin-coated onto the ITO and annealing at 160 °C for 10 min. The TB/L8-Bo, TB-F/L8-Bo and BTR-Cl/L8-Bo solutions were stirred at room temperature before spin-coating. And then, the donor/L8-Bo (different weight ratio) solution was spin-coated on the top of PEDOT:PSS from the chloroform (CF) solution. Then the ETL materials PDINO, PDINN, PNDIT-F3N were dissolved in methanol to a concentration of 1.0 mg/mL (for PNDIT-F3N, 0.3% acetic acid was added) and were spin-coated on top of the active layer (spinning rate: 2500 rpm for 30s). Finally, Ag (100 nm) was evaporated onto the active layer at a vacuum of  $\sim 2 \times 10^{-4}$  Pa to form the top electrode. The effective area of the device is 0.043 cm<sup>2</sup>. The current-voltage (*J-V*) characteristics were measured with a Keithley 2420 source measurement unit. The OSCs were measured under an irradiation intensity of 100 mW/cm<sup>2</sup> (AM 1.5 G) by a Newport solar simulator. The EQE spectra were analyzed using a certified Newport IPCE measurement system. The highly sensitive EQE was measured by using an integrated system (PECT-600, Enlitech), where the photocurrent was amplified and modulated by a lock-in instrument. Electroluminescence (EL) quantum efficiency (EQE<sub>EL</sub>) measurements were performed by applying external voltage/current sources through the devices (ELCT-3010, Enlitech).

**Table S4.** Detailed photovoltaic parameters of the BTR-Cl:L8-Bo devices with different CF SVA times

SVA time (s)	$V_{oc}$ (V)	$J_{sc}$ (mA/cm <sup>2</sup> )	FF	PCE (%)
20	0.93	23.02	56.2	12.0
30	0.92	23.26	63.2	13.6
40	0.92	22.22	62.76	12.8

**Table S5.** Detailed photovoltaic parameters of the BTR-Cl:L8-Bo devices with different CB SVA times

SVA time(s)	$V_{oc}$ (V)	$J_{sc}$ (mA/cm <sup>2</sup> )	FF	PCE (%)
20	0.89	21.80	51.3	10.1
30	0.86	23.72	73.0	15.0
40	0.86	22.17	69.6	13.5

**Table S6.** Photovoltaic parameters of the BTR-Cl:L8-Bo devices with different D/A ratios

D/A ratio	$V_{oc}$ (V)	$J_{sc}$ (mA/cm <sup>2</sup> )	FF	PCE (%)
1.2:1	0.87	23.36	71.5	14.5
1.4:1	0.86	23.69	73.0	14.9
1.6:1	0.86	23.76	70.4	14.4

**Table S7.** Detailed photovoltaic parameters of the TB:L8-Bo devices with different CF SVA times

SVA time (s)	$V_{oc}$ (V)	$J_{sc}$ (mA/cm <sup>2</sup> )	FF	PCE (%)
20	0.91	23.68	57.0	12.2
30	0.90	24.12	63.1	13.8
40	0.89	23.75	57.3	12.2

**Table S8.** Detailed photovoltaic parameters of the TB:L8-Bo devices with different CB SVA times

SVA time (s)	$V_{oc}$ (V)	$J_{sc}$ (mA/cm <sup>2</sup> )	FF	PCE (%)
20	0.88	24.09	67.1	14.3
30	0.86	24.67	74.5	15.6
40	0.86	23.03	74.5	14.7

**Table S9.** Photovoltaic parameters of the TB:L8-Bo devices with different D/A ratios

D/A ratio	$V_{oc}$ (V)	$J_{sc}$ (mA/cm <sup>2</sup> )	FF	PCE (%)
1.2:1	0.86	23.80	73.3	15.1
1.4:1	0.86	24.67	74.5	15.6
1.6:1	0.86	23.70	73.3	14.9

**Table S10.** Photovoltaic parameters of the TB:L8-Bo devices with different electron transport layers (ETL)

D/A ratio	ETL	$V_{oc}$ (V)	$J_{sc}$ (mA/cm <sup>2</sup> )	FF	PCE (%)
1.4:1	PDINN	0.86	23.59	74.1	15.0
1.4:1	PDINO	0.86	23.83	73.3	15.1
1.4:1	PNDIT-F3N	0.86	24.48	74.8	15.7

**Table S11.** Detailed photovoltaic parameters of the TB-F:L8-Bo devices with different CF SVA times

SVA time (s)	$V_{oc}$ (V)	$J_{sc}$ (mA/cm <sup>2</sup> )	FF	PCE (%)
20	0.92	23.72	62.9	13.7
30	0.92	24.05	67.0	14.8
40	0.91	23.36	66.1	14.1

**Table S12.** Detailed photovoltaic parameters of the TB-F:L8-Bo devices with different CB SVA times

SVA time (s)	$V_{oc}$ (V)	$J_{sc}$ (mA/cm <sup>2</sup> )	FF	PCE (%)
20	0.91	23.30	59.5	12.6
25	0.88	25.15	73.3	16.2
30	0.87	25.41	76.7	17.0
35	0.87	24.99	74.8	16.3
40	0.87	23.30	72.7	14.8

**Table S13.** Photovoltaic parameters of the TB-F:L8-Bo devices with different D/A ratios

D/A ratio	$V_{oc}$ (V)	$J_{sc}$ (mA/cm <sup>2</sup> )	FF	PCE (%)
1.2:1	0.87	25.01	74.1	16.0
1.4:1	0.87	25.26	75.6	16.6
1.6:1	0.87	24.83	72.3	15.7

**Table S14.** Photovoltaic parameters of the TB-F:L8-Bo devices with different electron transport layers (ETL)

D/A ratio	ETL	$V_{oc}$ (V)	$J_{sc}$ (mA/cm <sup>2</sup> )	FF	PCE (%)
1.4:1	PDINN	0.88	25.04	73.3	16.1
1.4:1	PDINO	0.87	24.27	75.2	15.9
1.4:1	PNDIT-F3N	0.87	25.45	74.8	16.6

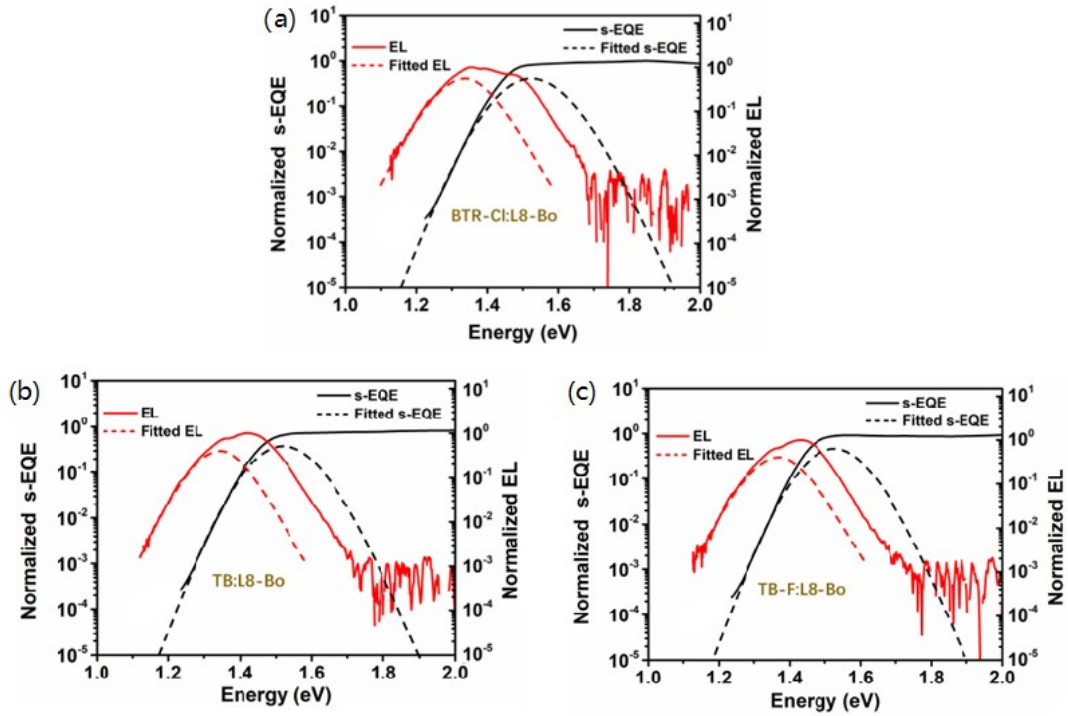


**Figure 30.** Semi-logarithmic plots of the EL (solid red lines), sensitive EQE (solid black lines) and reciprocally calculated EL and EQE (dashed lines) as a function of energy for OSCs for (a) BTR-Cl:L8-Bo, (b) TB:L8-Bo and (c) TB-F:L8-Bo.

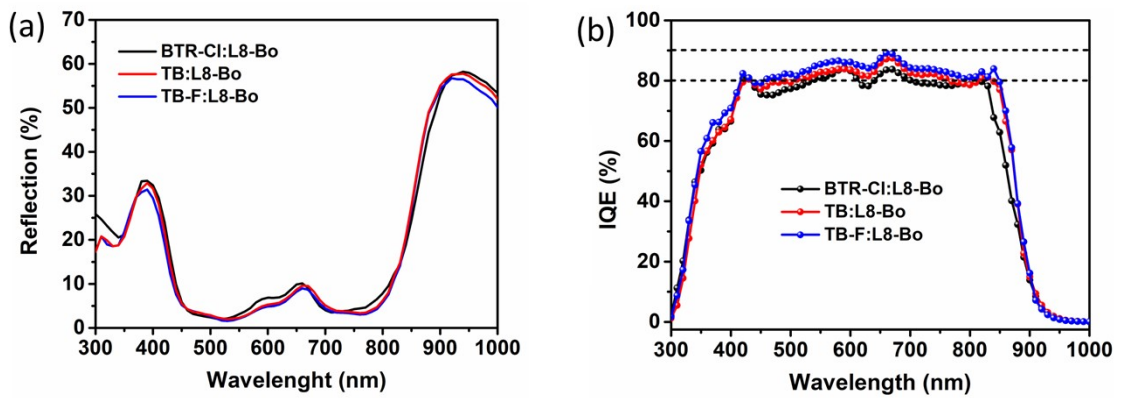


**Figure 31.** (a) Reflection curves of the BTR-Cl:L8-Bo, TB:L8-Bo and TB-F:L8-Bo-based devices. (b) IQE curves of the corresponding devices.

## 11. Space-Charge-Limited Current Measurements

The hole and electron mobilities were calculated using the space charge limited current (SCLC) model with a device configuration of ITO/PEDOT:PSS/active layer/MoO<sub>3</sub>/Ag and ITO/ZnO/active layer/PDINO/Ag, respectively, where the current density is calculated by:

$$J = 9\varepsilon_0\varepsilon_r\mu V^2/(8L^3)$$

where  $J$  stands for current density,  $\varepsilon_0$  is the permittivity of free space,  $\varepsilon_r$  is the relative dielectric constant of the transport medium,  $\mu$  is the hole mobility,  $V$  is the voltage drop across the device ( $V = V_{\text{appl}} - V_{\text{bi}} - V_{\text{RS}}$ , where  $V_{\text{appl}}$  is the applied voltage to the device,  $V_{\text{bi}}$  is the built-in voltage due to the difference in work function of the two electrodes, and  $V_{\text{RS}}$  is the voltage drop due to series resistance across the electrodes), and  $L$  is the thickness of the active layer.

**Table S15.** Summary of the fitting data for hole-only and electron-only device based on SMD:L8-Bo blends

Active layers	$\mu_{\text{h}}$ (cm <sup>2</sup> V <sup>-1</sup> s <sup>-1</sup> )	$\mu_{\text{e}}$ (cm <sup>2</sup> V <sup>-1</sup> s <sup>-1</sup> )	$\mu_{\text{h}}/\mu_{\text{e}}$
BTR-Cl	2.29×10 <sup>-4</sup>		
TB	3.18×10 <sup>-4</sup>		
TB-F	4.79×10 <sup>-4</sup>		
BTR-Cl:L8-Bo	2.03×10 <sup>-4</sup>	3.72×10 <sup>-4</sup>	0.55
TB:L8-Bo	3.65×10 <sup>-4</sup>	4.44×10 <sup>-4</sup>	0.83
TB-F:L8-Bo	4.79×10 <sup>-4</sup>	4.45×10 <sup>-4</sup>	1.08

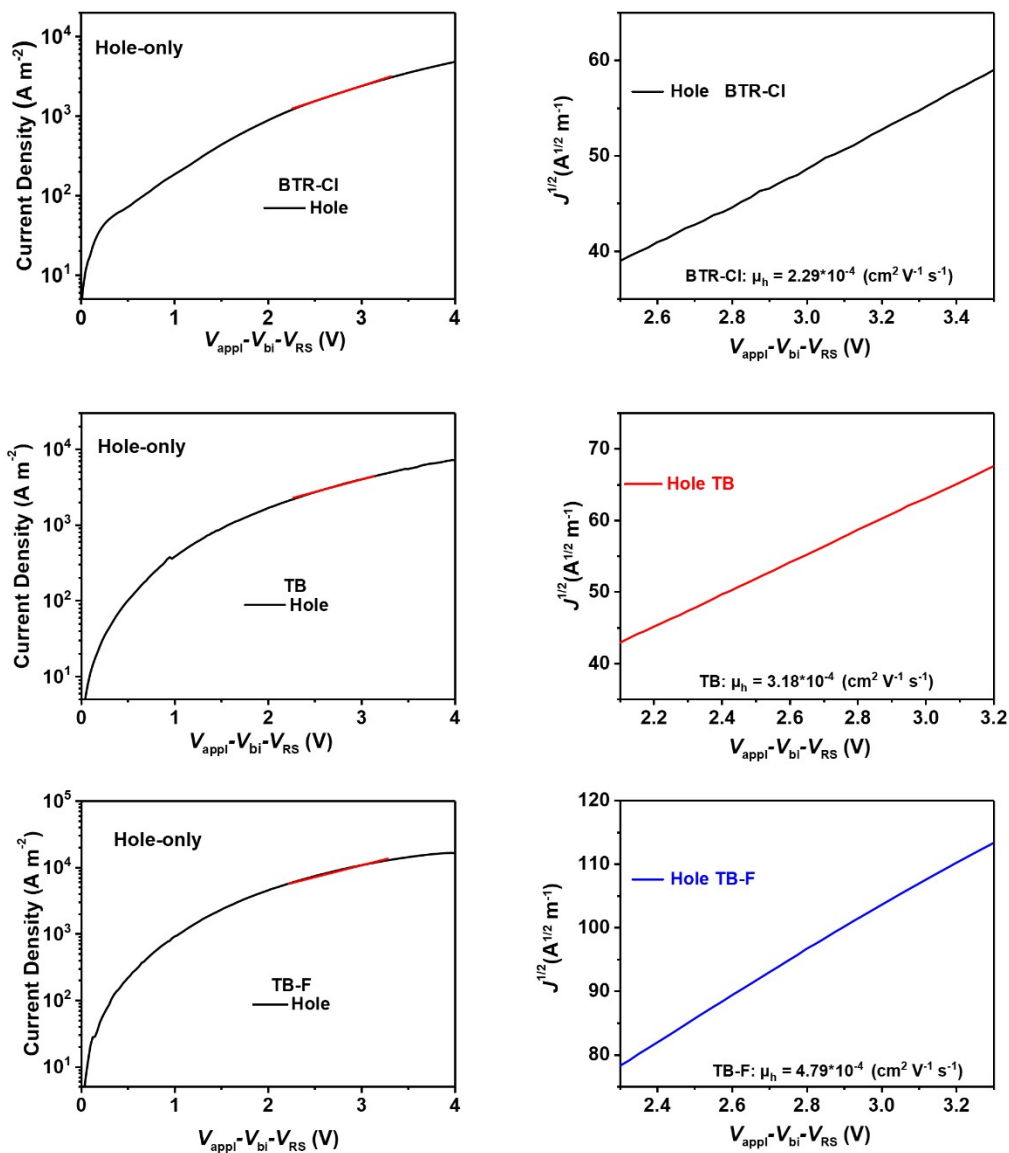
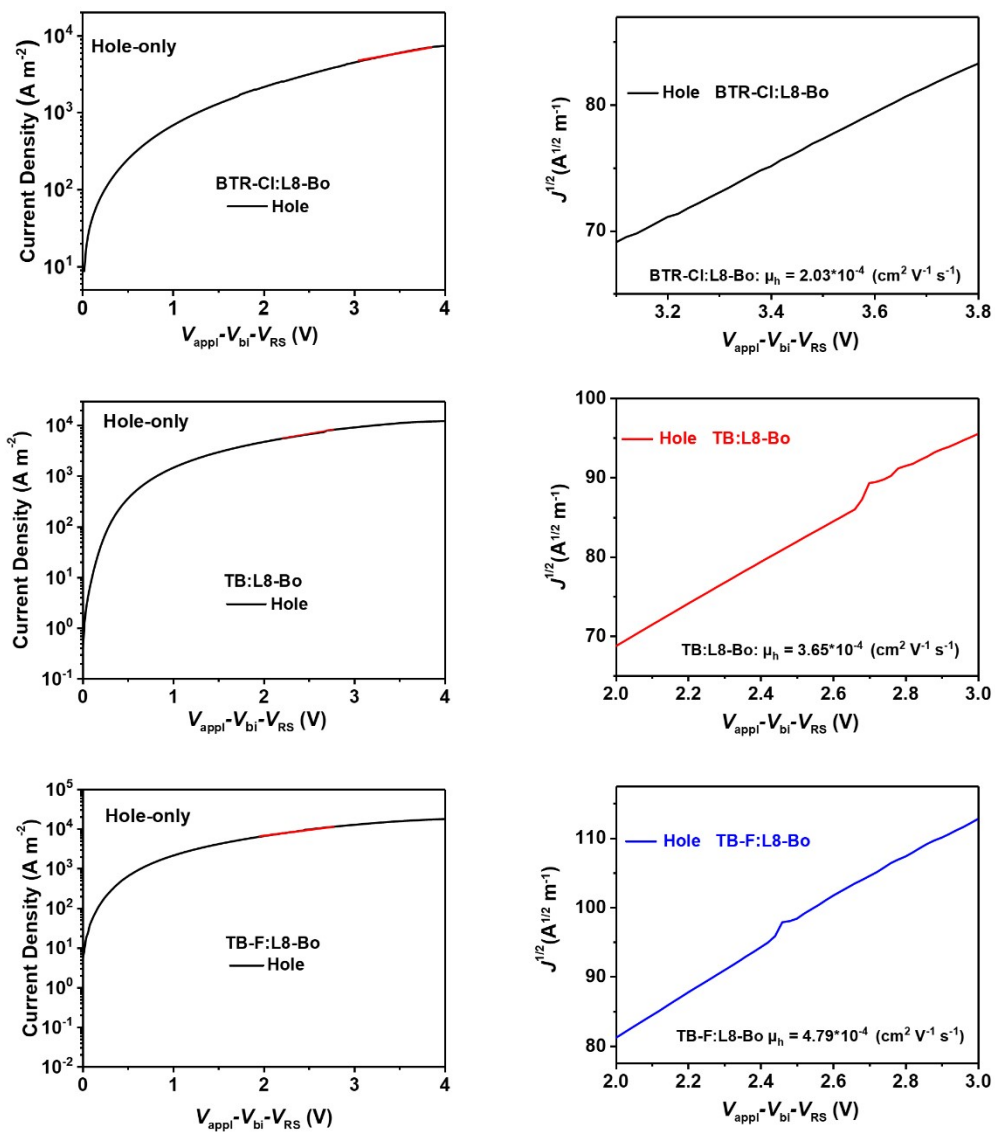


Figure S32. SCLC curves of hole-only devices of neat films.



**Figure S33.** SCLC curves of hole-only devices of the blend films.

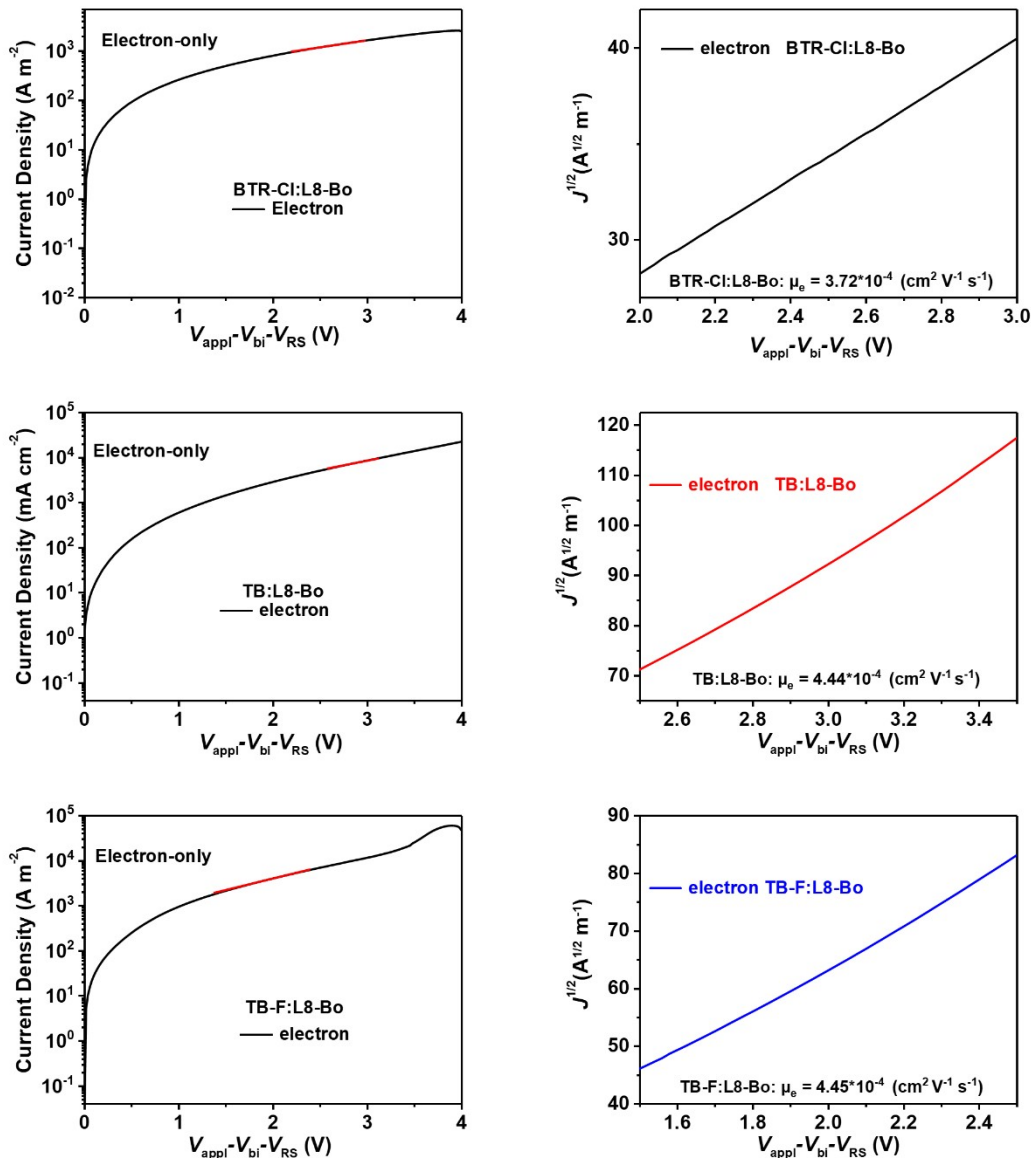


Figure S34. SCLC curves of electron-only devices of the blend films.

## 12. Dielectric constant Measurements

The Dielectric constants of SMD neat films were measured with a simple device structure of ITO/SMD/Ag at difference frequency from 10 Hz to 10M Hz. According to the previous work, the dielectric constant should be evaluated at the material's geometric capacitance, which represents the capacitance measured when the capacitance derives from only the material itself—the electronic, atomic, and ionic polarization.<sup>[28]</sup> The stable capacitive response with respect to frequency ranging from 10K HZ to 1M Hz is obtained. Relative dielectric constant ( $\epsilon_r$ ) can be calculated by the equation:

$$\epsilon_r = \frac{C_p \times d}{A \times \epsilon_0}$$

Where  $C_p$  is the measured capacitance;  $d$  is the thickness of film;  $A$  is the contact area and  $\epsilon_0$  is the permittivity of free space.

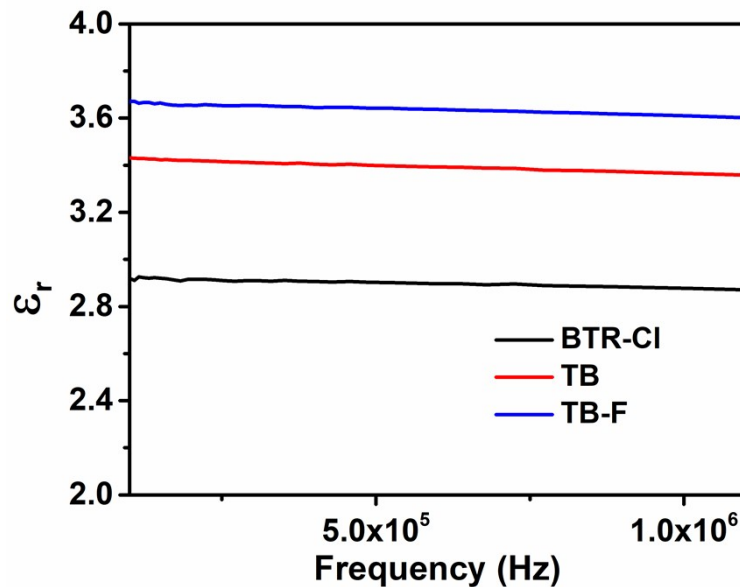


**Figure 35.** Relative dielectric constant ( $\epsilon_r$ ) as a function of frequency for SMDs neat and blend films.

### 13. Femtosecond Transient Absorption Spectroscopy Measurements

Femtosecond transient absorption spectroscopy measurements were performed on an Ultrafast Helios pump-probe system in collaboration with a regenerative amplified laser system from Coherent. An 800 nm pulse with a repetition rate of 1k Hz, a length of 100 fs, and an energy of 7 mJ pulse, was generated by an Ti:sapphire amplifier (Astrella, Coherent). Then the 800 nm pulse was separated into two parts by a beam splitter. One part was coupled into an optical parametric amplifier (TOPAS, Coherent) to generate the pump pulses at various wavelength. The other part was focused onto a sapphire plate and a YAG plate to generate white light supercontinuum as the probe beams with spectra covering 420-800 nm and 750-1400 nm, respectively. The time delay between pump and probe was controlled by a motorized optical delay line with a maximum delay time of 8 ns. The pump pulse is chopped by a mechanical chopper with 500 Hz and then focused on to the mounted sample with probe beams. The probe beam was collimated and focused into a fiber-coupled multichannel spectrometer with CCD sensor. The energy of pump pulse was measured and calibrated by a power meter (PM400, Thorlabs). The samples used for TA measurements were obtained by spin-coating the neat and blend solutions on the quartz substrates.

#### The detailed calculation processes of exciton diffusion length

Multi-exponential fitting method was used to fit the exciton lifetimes.

The used equations are shown as follows:

$$I_{(t)} = A_1 e^{-\frac{t}{\tau_1}} + A_2 e^{-\frac{t}{\tau_2}} + A_3 e^{-\frac{t}{\tau_3}}$$
$$\tau = A_1 \times \tau_1 + A_2 \times \tau_2 + A_3 \times \tau_3$$

Where  $A_i$  is the proportion of the corresponding lifetime of  $\tau_i$ .

The thicknesses of BTR-Cl:L8-Bo and TB-F:L8-Bo films are approximately 101, 109 nm. Exciton-exciton annihilation (EEA) method considers that there are two main quenching channels for excitons, radiative and non-radiative deactivations with trap-induced recombination lifetime constant ( $k$ ) and bimolecular EEA with a bimolecular decay rate coefficient ( $\gamma$ ).<sup>[29]</sup> The relationship is shown as follows:

$$-\frac{dn(t)}{dt} = kn(t) + \gamma n^2(t)$$

$$n(t) = \frac{n(0)\exp\left[-\frac{\gamma n(0)t}{k}\right]}{1 + \frac{\gamma}{k}n(0)[1 - \exp\left(-\frac{\gamma n(0)t}{k}\right)]}$$

Where  $n(t)$  is the exciton density at a decay time of  $t$ . In order to calculate  $k$ , a low excitation intensity of  $0.2 \mu\text{J cm}^{-2}$  was used to ensure that EEA effect was absent in the films. The 2D images and corresponding decay profiles of excitons in BTR-Cl and TB-F phases are shown in **Figure S37** and **Figure S38**. Photoexcitation of pure BTR-Cl, TB-F and corresponding blend films at 460 nm results in the appearance of a broad ground state bleaching (GSB) signals. In addition, as expected, the decay kinetics are approximately single exponential decay function at low excitation intensities, which obey the following equation:

$$\frac{dn(t)}{dt} = -kn(t)$$

When the exciton concentrations decay to 1/2 of the original values at low excitation densities, the solution of the equation is a single exponential decay function. The lifetime of BTR-Cl, TB-F GSB kinetics in blend films is 338 and 225 ps, respectively. Therefore, the corresponding  $k$  values are  $2.1 \times 10^9$  and  $3.1 \times 10^9 \text{ s}^{-1}$ , as shown in **Table S16**.

On the other hand, EEA effect occurs when a relatively high excitation intensity is used, which leads to obviously different decay dynamics, and we can obtain the equations as follows:

$$t_{1/2} = \frac{a \ln 2}{k}, a < 1$$

$$\gamma = \frac{k(2\exp(-a \ln 2) - 1)}{n_0(1 - \exp(-a \ln 2))}$$

If the value of  $a$  is low enough, we can consider that  $\exp(-a \ln 2) = 1 - a \ln 2$ . Then the above equation can be equivalent to:

$$\gamma = \frac{k(1 - 2a \ln 2)}{n_0 a \ln 2}$$

When the excitation power density is  $30 \mu\text{J cm}^{-2}$ , the calculated values of  $\gamma$  are  $0.95 \times 10^{-9}$ ,  $2.43 \times 10^{-9} \text{ cm}^3 \text{ s}^{-1}$  and  $2.66 \times 10^{-9} \text{ cm}^3 \text{ s}^{-1}$  for BTR-Cl and TB-F phases.

Then, the diffusion coefficient  $D$  can be obtained through the following equation:

$$D = \frac{\gamma}{4\pi R}$$

where  $R$  is the annihilation radius of singlet excitons.  $R$  is assumed to be 2

nm.<sup>[30]</sup> The exciton diffusion length can be calculated by the following equation<sup>7</sup>:

$$L_D = \sqrt{\frac{D}{k_1}}$$

Note that the difference in exciton diffusion length is mainly due to the various exciton diffusion coefficients, which corresponds to the diffusion rate.<sup>[31]</sup>

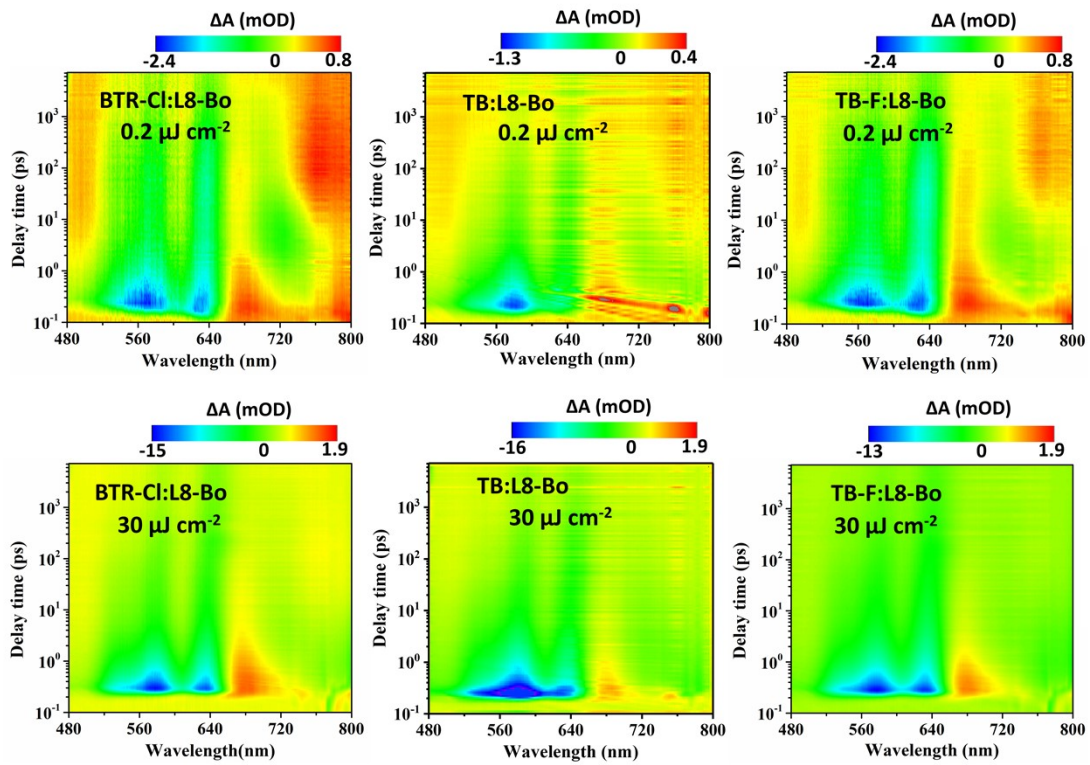


**Figure S36.** The TA images of BTR-Cl:L8-Bo, TB:L8-Bo and TB-F:L8-Bo films under the excitation of 460 nm with different energy of pulse ( $0.2 \mu\text{J cm}^{-2}$  and  $30 \mu\text{J cm}^{-2}$ ).

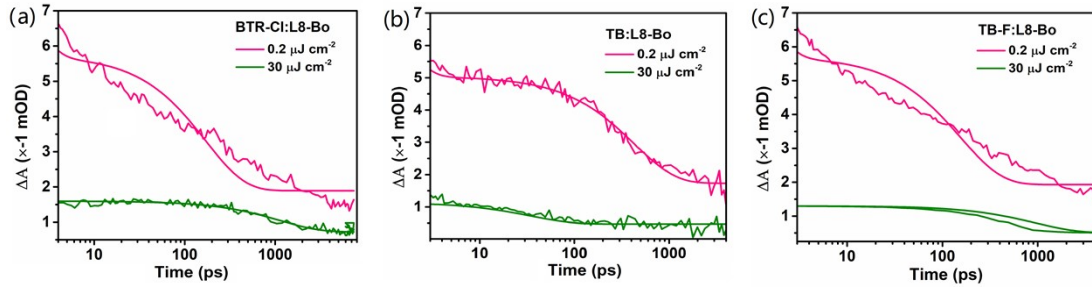


**Figure S37.** Singlet exciton decay dynamics with different excitation wavelength: (a) in BTR-Cl:L8-Bo film under the excitation of 460 nm, 0.2 and 30  $\mu\text{J cm}^{-2}$ ; (b) in TB:L8-Bo film under the excitation of 460 nm, 0.2 and 30  $\mu\text{J cm}^{-2}$ ; (c) in TB-F:L8-Bo film under the excitation of 460 nm, 0.2 and 30  $\mu\text{J cm}^{-2}$ .

**Table S16. Detailed parameters of single exciton decay dynamic for blend films**

Materials	Pump energy ( $\mu\text{J cm}^{-2}$ )	$n_0$ ( $\times 10^{18} \text{ cm}^{-3}$ )	$t_{1/2}$ (ps)	$k$ ( $\times 10^9 \text{ s}^{-1}$ )	$a$	$\gamma$ ( $\times 10^{-9} \text{ cm}^{-2} \text{ s}^{-1}$ )	$D$ ( $\times 10^{-4} \text{ cm}^{-2} \text{ s}^{-1}$ )	$L_D$ (nm)
BTR-Cl/L8-Bo	0.2	0.062	338	2.1				
	30	9.47	76		0.23	0.95	3.77	4.23
TB/L8-Bo	0.2	0.060	248	2.8				
	30	9.31	45		0.18	1.83	7.01	5.10
TB-F/L8-Bo	0.2	0.058	225	3.1				
	30	8.85	34		0.15	2.66	10.57	5.84

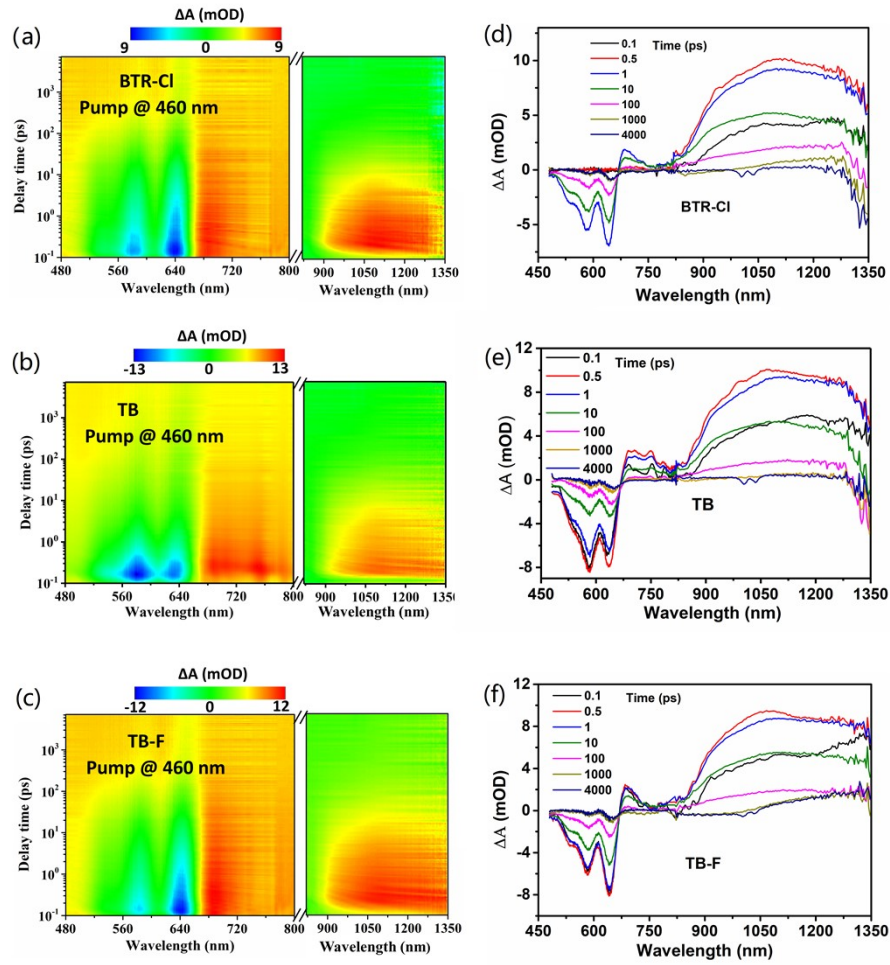


**Figure 38.** Color plots of the TA spectra in the range of 480-800 nm and 820-1350 nm of (a) BTR-Cl, (b) TB and (c) TB-F neat film under 460 nm excitation. TA spectra in the range of 480-800 nm and 820-1350 nm of (d) BTR-Cl, (e) TB and (f) TB-F neat film under 460 nm at different delay times.

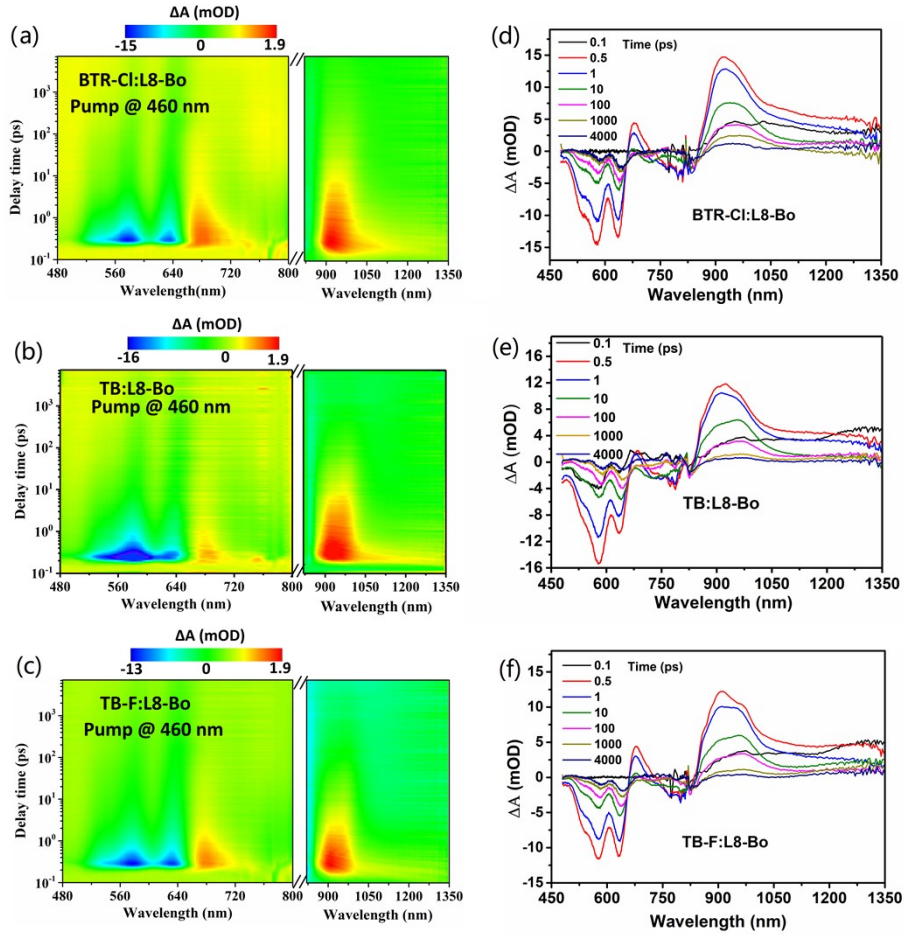


**Figure 39.** Color plots of the TA spectra in the range of 480-800 nm and 820-1350 nm of (a) BTR-CI:L8-Bo and (b) TB:L8-Bo and (c) TB-F:L8-Bo blend film under 460 nm excitation. TA spectra in the range of 480-800 nm and 820-1350 nm of (d) BTR-CI:L8-Bo, (e) TB:L8-Bo and (f) TB-F:L8-Bo blend film under 460 nm at different delay times.

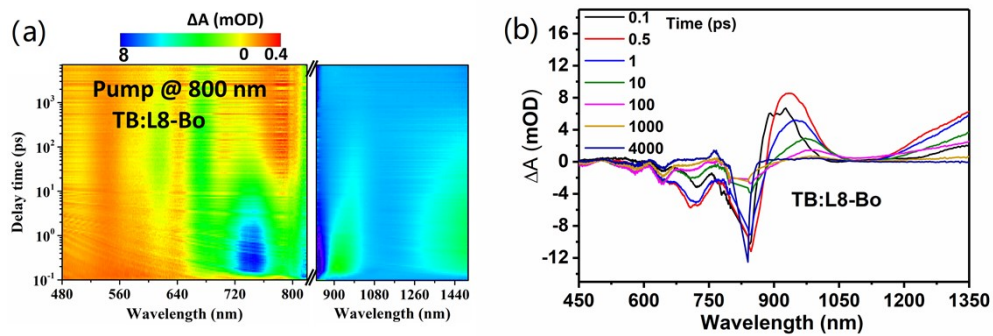


**Figure 40.** Color plots of the TA spectra in the range of 480-800 nm and 820-1350 nm of TB:L8-Bo blend film under 800 nm excitation. TA spectra in the range of 480-800 nm and 820-1350 nm of (b) TB:L8-Bo blend film under 800 nm at different delay times.

## **14. Atomic Force Microscopy**

Standard tapping-mode AFM measurements in ambient were performed on a Scanned Probe Imaging and Development (SPID) on Park NX-10. The AFM images were confirmed from different samples and scan areas. The root-mean-square roughness (RMS) values of height images were obtained from the whole scan area ( $5\ \mu\text{m} \times 5\ \mu\text{m}$ ). All the AFM images were flattened and exported from the software.

## **15. Transmission Electronic Microscopy**

The detailed experimental procedure followed our previous report. First, a layer of PEDOT:PSS was spin coated (rate = 5000 rpm) on top of a pre-cleaned ITO slide. The obtained PEDOT:PSS/ITO substrate thermally annealed at 150 °C for 15 min. Then the BHJ coating solution with the optimized device fabrication condition (D:A mass ratio = 1.4:1 with SVA treatment for 30 s; total organic concentration = 20 mg/mL) was spin coated (rate = 2000 rpm) on top of the annealed PEDOT:PSS/ITO substrates. The obtained organics/PEDOT:PSS/glass substrates were then immersed into deionized water at room temperature, and after several minutes, the BHJ blend films exfoliated from the glass substrate. The floated single-layer organic blend films were transferred to transmission electron microscopy (TEM) copper grids.

## 16. Binding Energy and D/A Molecular Stacking Calculation

All-electron DFT calculations have been carried out by the latest version of ORCA quantum chemistry software<sup>[32]</sup> (Version 5.0.1).

The BLYP function<sup>[33]</sup> was adopted for all calculations. For geometry optimization calculations, the def2SVP basis set<sup>[34]</sup> was used. The DFT-D3 with BJ-damping<sup>[35]</sup> was applied to correct the weak interaction to improve the calculation accuracy. The nature of noncovalent interaction was studied by using IGM (Independent Gradient Model) method through Multiwfn software.<sup>[36]</sup> The visualization of IGM and orbitals were rendered by VMD.<sup>[37]</sup>

The binding energy between molecule donor and acceptor was calculated by the following formula:  $E_{\text{binding}} = E_{\text{complex}} - (E_{\text{partA}} + E_{\text{partB}})$ .

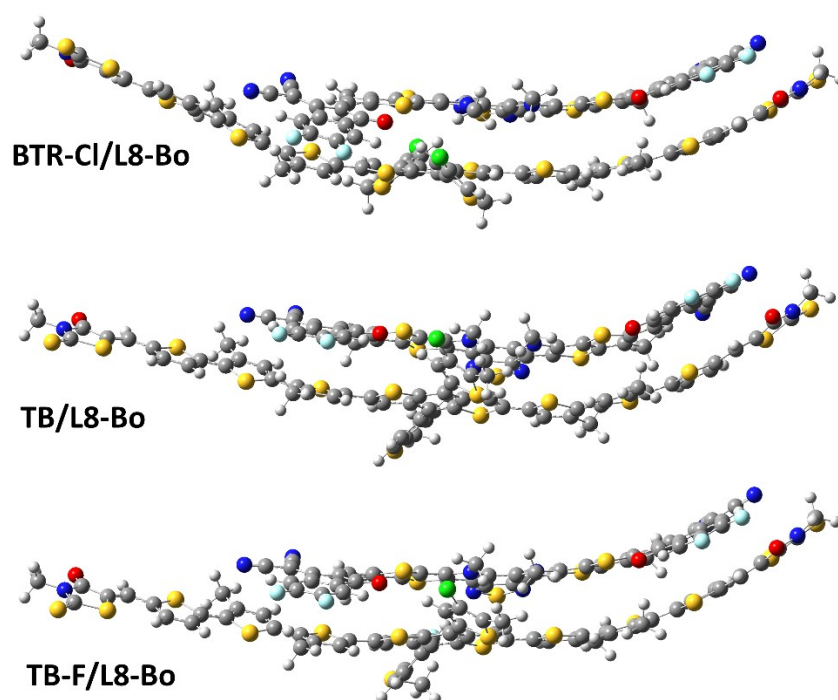


**Figure S41.** The optimized molecular stacking of the three donor/acceptor systems.

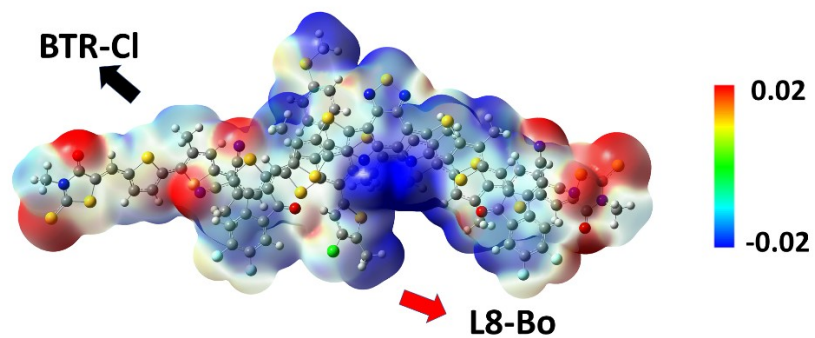


**Figure S42.** The ESP distributions of BTR-Cl/L8-Bo system under optimized conformation.

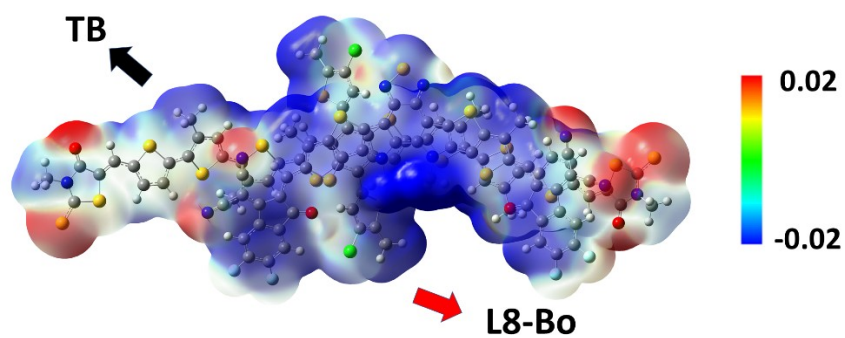


**Figure S43.** The ESP distributions of TB/L8-Bo system under optimized conformation.

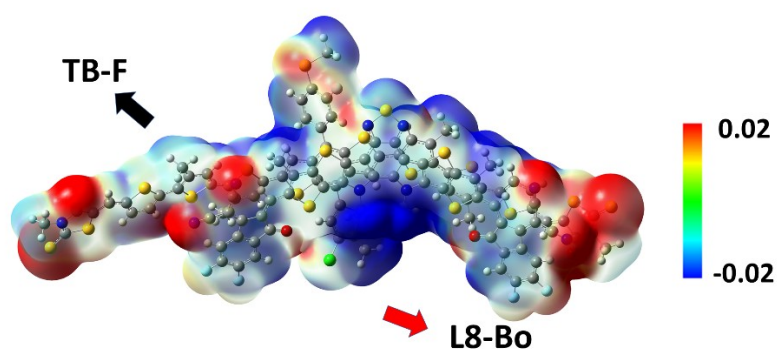


**Figure S44.** The ESP distributions of TB-F/L8-Bo system under optimized conformation.

**Table S17.** The total energies and interaction energies for optimized conformations

<b>D/A system</b>		<b>Total energy (Hartree)</b>	<b>Binding energy (kJ/mol)</b>	<b>Binding energy (kcal/mol)</b>
<b>BTR-Cl/L8- Bo</b>	<b>Complex</b>	-13799.30898		
	<b>BTR-Cl</b>	-8983.720112	-413.5661492	-98.8447512
	<b>L8-Bo</b>	-4815.431344		
<b>TB:L8-Bo</b>	<b>Complex</b>	-13417.19473		
	<b>TB</b>	-8601.598817	-433.9089061	-103.7067902
	<b>L8-Bo</b>	-4815.430643		
<b>TB-F/L8-Bo</b>	<b>Complex</b>	-13516.35287		
	<b>TB-F</b>	-8700.756729	-436.9657477	-104.4373934
	<b>L8-Bo</b>	-4815.429712		

## 17. In-depth X-ray Photoelectron Spectroscopy Measurement

In this experiment, in-depth XPS measurements were conducted on a ThermoFischer, ESCALAB Xi+ instrument. The pressure in analysis room is  $8 \times 10^{-10}$  Pa. The excitation source is Al Ka ray ( $h\nu = 1486.6$  eV). The working voltage is 12.5 kV and the filament current is 16 mA. The test passing-energy is 100 eV in full spectrum and 20 eV in narrow spectrum, with step size of 0.05 eV and stay time of 40-50 ms.

Etching conditions: The sample was etched and thinned with an argon ion gun, the etching spot size was 1.5 mm, and the etching voltage was 3000 eV.

For the SMDs:L8-Bo system, only Cl can be used for the acceptor detection. As the three blends of BTR-Cl:L8-Bo, TB:L8-Bo, and TB-F:L8-Bo measured in this experiment are structurally very similar and the ion-beam emission parameters are the same for each measurement, and the applied etching rate is essentially same. All the sample films were spin-coated on ITO/PEDOT glass substrates in a glovebox, using the same conditions as the optimized OSC devices.

Calculation Procedures:

For BTR-Cl:L8-Bo, TB:L8-Bo and TB-F:L8-Bo, the optimized weight ratio (D: A) = 1.4:1. As the molecular weights of BTR-Cl, TB, TB-F and L8-Bo are 1929, 1922, 1940 and 1484, the converting mole ratios of ideal D:A are 1.077, 1.081, 1.071, respectively. Thus, the ideal D:(A+D) mole ratios are 0.518 for BTR-Cl:L8-Bo, 0.519 for TB:L8-Bo and 0.517 for TB-F:L8-Bo, respectively.

For BTR-Cl:L8-Bo, the D:(A+D) mole ratios measured from XPS can be carried out by:

$$14a + 5b = S \text{ (measured from XPS)}$$

$$102a + 84b = C \text{ (measured from XPS)}$$

$$D:(A + D) \text{ mole ratios measured from XPS} = \frac{a(\text{donor})}{a(\text{donor}) + b(\text{acceptor})}$$

The deviation factor represents the miscibility properties of D/A couple.

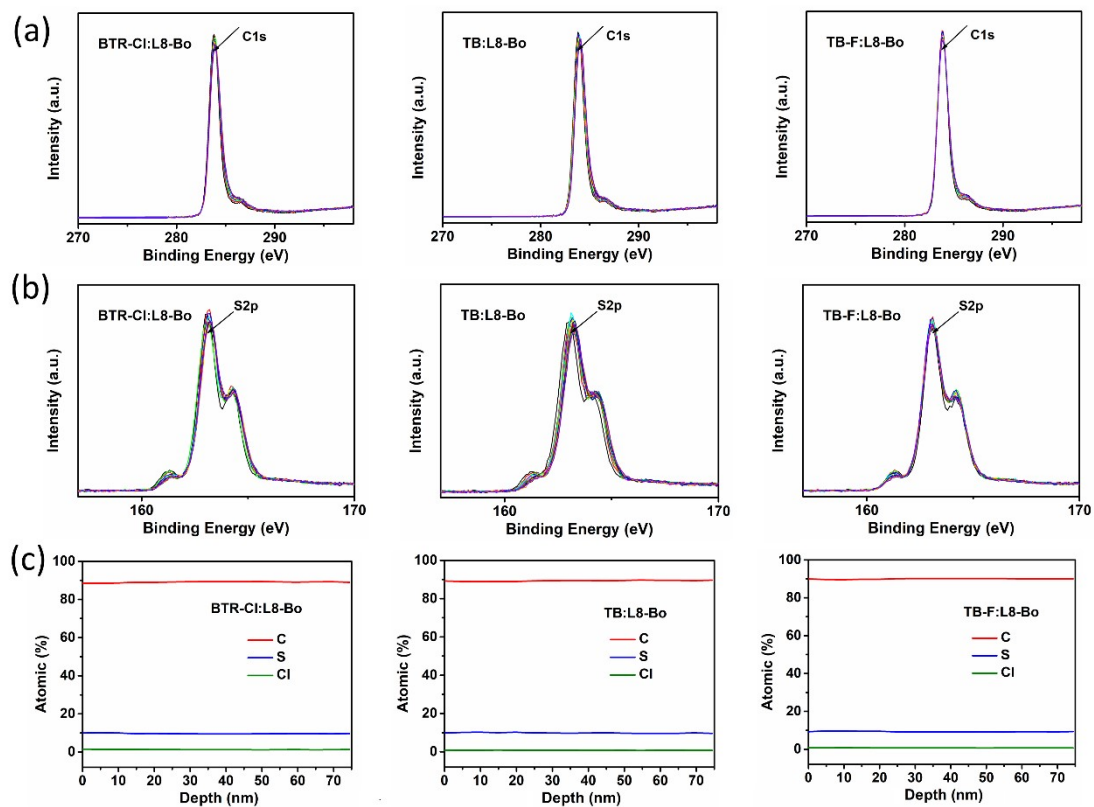


**Figure S45.** Vertical morphologies of blend films. (a) Depth C1s profiles of XPS data, (b) depth S2p profiles of XPS data, and (c) atomic combination of BTR-Cl:L8-Bo, TB:L8-Bo and TB-F:L8-Bo based on ITO/PEDOT:PSS substrates.

## 18. Molecular Dynamic Analysis

All the all-atom MD simulations were based on a AMBER force field [38] with the RESP charges, [39] and were carried out using the Gromacs-4.6.7 software package.[40] The time step was 2 fs, and the total run time was 20 ns NPT for the equilibrium MD simulation. The thin-films were built and imitated using the following procedure:

- (1) Randomly placing total 140:100 molecules in a  $18 \times 18 \times 18$  nm<sup>3</sup> box to generate an initial geometry;
- (2) 5 ns of simulation at 800 K and 100 bar to make molecules close together quickly;
- (3) 10 ns of simulation at 800 K and 1 bar, then cooling down to 300 K in 5 ns;
- (4) 10 ns of equilibration at 300 K and 1 bar (equilibration).

The velocity rescaling thermostat and the Berendsen barostat under the NPT ensemble were applied to control the temperature and pressure, respectively [41, 42]. But for the final 10 ns of equilibration, the Nosé-Hoover thermostat and the Parrinello-Rahman barostat were used to obtain better equilibrium conformations. [43, 44] The Particle Mesh-Ewald method [45-47] was used to compute long-range electrostatics within a relative tolerance of  $1 \times 10^{-6}$ . A cut-off distance of 1.2 nm was applied to real-space Ewald interactions. The same value was used for van der Waals interactions. The LINCS algorithm [48] was applied to constrain bond lengths of hydrogen atoms. A leap-frog algorithm [49] was used with a time step of 2 fs.

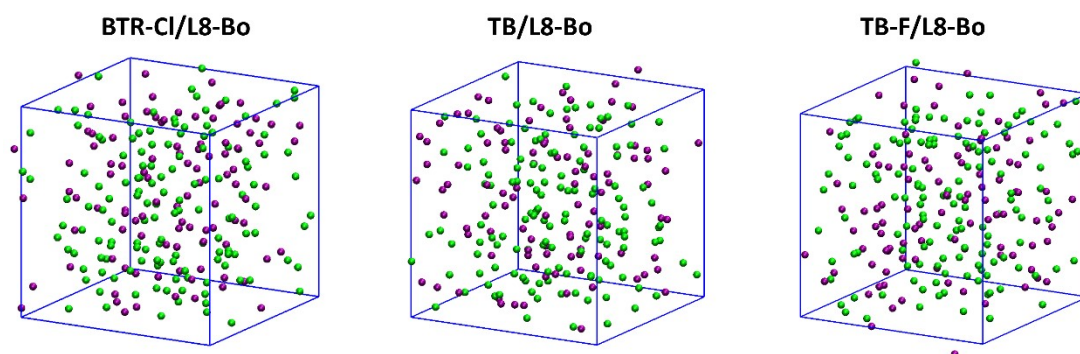


**Figure S46.** Molecule distribution from MD simulation. The green ball represents the small molecular donor, and the purple ball for acceptor L8-Bo.

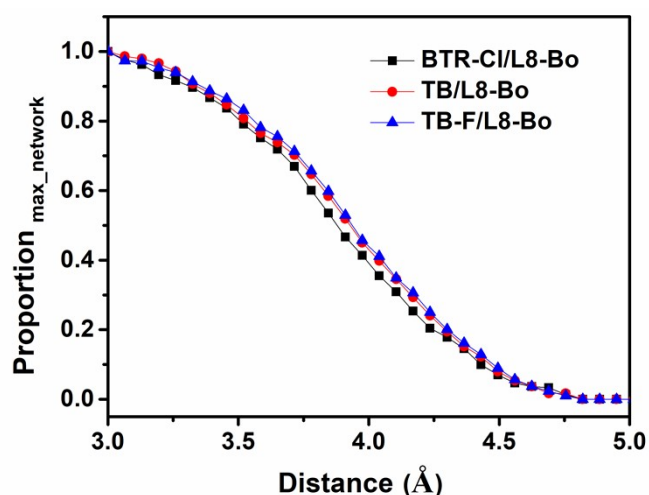


**Figure S47.** Proportion of the number of molecules in the largest connection network over the total number of molecules in the film, as a function of the intermolecular distance for the three blend films.

## Reference

- [1] Y. Gao, Z. Shen, F. Tan, G. Yue, R. Liu, Z. Wang, S. Qu, Z. Wang, W. Zhang, *Nano Energy* **2020**, *76*, 104964.
- [2] Q. Yue, H. Wu, Z. Zhou, M. Zhang, F. Liu, X. Zhu, *Adv. Mater.* **2019**, *31*, 1904283.
- [3] R. Zhou, Z. Jiang, C. Yang, J. Yu, J. Feng, M. A. Adil, D. Deng, W. Zou, J. Zhang, K. Lu, W. Ma, F. Gao, Z. Wei, *Nat. Commun.* **2019**, *10*, 5393.
- [4] H. Chen, D. Hu, Q. Yang, J. Gao, J. Fu, K. Yang, H. He, S. Chen, Z. Kan, T. Duan, C. Yang, J. Ouyang, Z. Xiao, K. Sun, S. Lu, *Joule* **2019**, *3*, 3034.
- [5] H. Tang, H. Chen, C. Yan, J. Huang, P. W. K. Fong, J. Lv, D. Hu, R. Singh, M. Kumar, Z. Xiao, Z. Kan, S. Lu, G. Li, *Adv. Energy Mater.* **2020**, *10*, 2001076 .
- [6] J. Ge, L. Xie, R. Peng, B. Fanady, J. Huang, W. Song, T. Yan, W. Zhang, Z. Ge, *Angew. Chem. Int. Ed.* **2020**, *59*, 2808.
- [7] Y. Wang, Y. Wang, L. Zhu, H. Liu, J. Fang, X. Guo, F. Liu, Z. Tang, M. Zhang, Y. Li, *Energy Environ. Sci.* **2020**, *13*, 1309.
- [8] J. Gao, J. Ge, R. Peng, C. Liu, L. Cao, D. Zhang, B. Fanady, L. Hong, E. Zhou, Z.

- Ge, *J. Mater. Chem. A* **2020**, *8*, 7405.
- [9] J. Ge, L. Hong, W. Song, L. Xie, J. Zhang, Z. Chen, K. Yu, R. Peng, X. Zhang, Z. Ge, *Adv. Energy Mater.* **2021**, *11*, 2100800.
- [10] B. Qiu, Z. Chen, S. Qin, J. Yao, W. Huang, L. Meng, H. Zhu, Y. M. Yang, Z. G. Zhang, Y. Li, *Adv. Mater.* **2020**, *32*, 1908373.
- [11] J. Qin, C. An, J. Zhang, K. Ma, Y. Yang, T. Zhang, S. Li, K. Xian, Y. Cui, Y. Tang, W. Ma, H. Yao, S. Zhang, B. Xu, C. He, J. Hou, *Sci. China Mater.* **2020**, *63*, 1142.
- [12] M. Jiang, H.-r. Bai, H.-f. Zhi, J.-k. Sun, J.-l. Wang, F. Zhang, Q. An, *ACS Energy Lett.* **2021**, *6*, 2898.
- [13] R. Sun, Y. Wu, J. Guo, Z. Luo, C. Yang, J. Min, *Sci. China Chem* **2020**, *63*, 1246.
- [14] X. Wang, J. Wang, J. Han, D. Huang, P. Wang, L. Zhou, C. Yang, X. Bao, R. Yang, *Nano Energy* **2021**, *81*, 105612.
- [15] X. Wang, D. Huang, J. Han, L. Hu, C. Xiao, Z. Li, R. Yang, *ACS Appl. Mater. Interfaces* **2021**, *13*, 11108.
- [16] R. Zhou, Z. Jiang, Y. Shi, Q. Wu, C. Yang, J. Zhang, K. Lu, Z. Wei, *Adv. Funct. Mater.* **2020**, *30*, 2005426.
- [17] J. Guo, B. Qiu, D. Yang, C. Zhu, L. Zhou, C. Su, U. S. Jeng, X. Xia, X. Lu, L. Meng, Z. Zhang, Y. Li, *Adv. Funct. Mater.* **2021**, *32*, 2110159.
- [18] Y. Wang, Q. Fan, Y. Wang, J. Fang, Q. Liu, L. Zhu, J. Qiu, X. Guo, F. Liu, W. Su, M. Zhang, *Chin. J. Chem.* **2021**, *39*, 2147.
- [19] C. Hu, J. Xu, S. Cai, P. Huang, J. Oh, C. Yang, S. Chen, K. Sun, K. Yang, S. Lu, *Sol. RRL* **2021**, *5*, 2100705.
- [20] W. Su, Y. Wang, Z. Yin, Q. Fan, X. Guo, L. Yu, Y. Li, L. Hou, M. Zhang, Q. Peng, Y. Li, E. Wang, *ChemSusChem* **2021**, *14*, 3535.
- [21] T. Xu, J. Lv, K. Yang, Y. He, Q. Yang, H. Chen, Q. Chen, Z. Liao, Z. Kan, T. Duan, K. Sun, J. Ouyang, S. Lu, *Energy Environ. Sci.* **2021**, *14*, 5366.
- [22] L. Zhang, X. Zhu, D. Deng, Z. Wang, Z. Zhang, Y. Li, J. Zhang, K. Lv, L. Liu, X. Zhang, H. Zhou, H. Ade, Z. Wei, *Adv. Mater* **2022**, *34*, 2106316.
- [23] S. Cai, P. Huang, G. Cai, X. Lu, D. Hu, C. Hu, S. Lu, *ACS Appl. Mater. Interfaces*

**2022**, *14*, 14532.

[24] L. Meng, M. Li, G. Lu, Z. Shen, S. Wu, H. Liang, Z. Li, G. Lu, Z. Yao, C. Li, X. Wan, Y. Chen, *Small* **2022**, 2201400.

[25] H. Liang, Y. Wang, X. Guo, D. Yang, X. Xia, J. Wang, L. Zhang, Y. Shi, X. Lu, M. Zhang, *J Mater. Chem. A* **2022**, *10*, 10926.

[26] J. Ge, L. Hong, H. Ma, Q. Ye, Y. Chen, L. Xie, W. Song, D. Li, Z. Chen, K. Yu, J. Zhang, Z. Wei, F. Huang, Z. Ge, *Adv. Mater* **2022**, 2202752.

[27] Y. Chang, X. Zhu, Y. Shi, Y. Liu, K. Meng, Y. Li, J. Xue, L. Zhu, J. Zhang, H. Zhou, W. Ma, Z. Wei, K. Lu, *Energy Environ. Sci.* **2022**, doi.org/10.1039/D2EE00726F

[28] M. P. Hughes, K. D. Rosenthal, N. A. Ran, M. Seifrid, G. C. Bazan, T. Q. Nguyen, *Adv. Funct. Mater.* **2018**, *28*, 1801542.

[29] H. Cha, S. Wheeler, S. Holliday, S. D. Dimitrov, A. Wadsworth, H. H. Lee, D. Baran, I. McCulloch, J. R. Durrant, *Adv. Funct. Mater.* **2018**, *28*, 1704389.

[30] P. Bi, S. Zhang, Z. Chen, Y. Xu, Y. Cui, T. Zhang, J. Ren, J. Qin, L. Hong, X. Hao, J. Hou, *Joule*, **2021**, *5*, 2408.

[31] O. Mikhnenko, P. Blom, T.-Q. T. Nguyen, *Energy Environ. Sci.*, **2015**, *8*, 1867.

[32] F. Neese, *WIREs Comput. Mol. Sci.* **2017**, *8*, 1327.

[33] Becke, D. Axel, *J. Chem. Phys.* **1992**, *96*, 2155.

[34] F. Weigend, R. Ahlrichs, *Phys. Chem. Chem. Phys.* **2005**, *7*, 3297.

[35] S. Grimme, S. Ehrlich, L. Goerigk, *J. Comput. Chem.* **2011**, *32*, 1456.

[36] S. Grimme, J. Antony, S. Ehrlich, H. Krieg, *J. Chem. Phys.* **2010**, *132*, 154104.

[37] T. Lu, F. Chen, *J. Comput. Chem.* **2012**, *33*, 580.

[38] J. Wang, R. M. Wolf, J. W. Caldwell, P. A. Kollman and D. A. Case, *J. Comput. Chem.*, **2004**, *25*, 1157.

[39] C. I. Bayly, P. Cieplak, W. Cornell, P. A. Kollman, *J. Phys. Chem.*, **1993**, *97*, 10269.

[40] B. Hess, C. Kutzner, D. van der Spoel and E. Lindahl, *J. Chem. Theory Comput.*, **2008**, *4*, 435.

[41] H. J. C. Berendsen, J. P. M. Postma, W. F. van Gunsteren, A. DiNola J. R. Haak, *J. Chem. Phys.*, **1984**, *81*, 3684.

- [42] S. Nosé, *J. Chem. Phys.*, **1984**, *81*, 511.
- [43] W. G. Hoover, *Physical Review A*, **1985**, *31*, 1695.
- [44] M. Parrinello and A. Rahman, *J. Appl. Phys.*, **1981**, *52*, 7182.
- [45] U. Essmann, L. Perera, M. L. Berkowitz, T. Darden, H. Lee, L. G. Pedersen, *J. Chem. Phys.* **1995**, *103*, 8577.
- [46] L. G. Astrakas, C. Gousias, M. Tzaphlidou, *J. Appl. Phys.* **2012**, *111*, 074702.
- [47] B. Hess, H. Bekker, H. J. Berendsen, J. G. Fraaije, *J. Comput. Chem.* **1997**, *18*, 1463.
- [48] W. F. Van Gunsteren, H. Berendsen, *Mol. Simul.* **1988**, *1*, 173.
- [49] G. Bussi, D. Donadio, M. Parrinello, *J. Chem. Phys.*, **2007**, *126*, 014101.